Contrib Mineral Petrol (2002) 144: 185–205
DOI 10.1007/s00410-002-0371-8

Ilya N. Bindeman · John W. Valley

Oxygen isotope study of the Long Valley magma system, California: isotope thermometry and convection in large silicic magma bodies

Received: 28 September 2001 / Accepted: 1 May 2002 / Published online: 10 July 2002

Abstract Products of voluminous pyroclastic eruptions with eruptive draw-down of several kilometers provide a snap-shot view of batholith-scale magma chambers, and quench pre-eruptive isotopic fractionations (i.e., temperatures) between minerals. We report analyses of oxygen isotope ratio in individual quartz phenocrysts and concentrates of magnetite, pyroxene, and zircon from individual pumice clasts of ignimbrite and fall units of caldera-forming 0.76 Ma Bishop Tuff (BT), pre-caldera Glass Mountain (2.1–0.78 Ma), and post-caldera rhyolites (0.65–0.04 Ma) to characterize the long-lived, batholith-scale magma chamber beneath Long Valley Caldera in California. Values of $\delta^{18}O$ show a subtle 1‰ decrease from the oldest Glass Mountain lavas to the youngest post-caldera rhyolites. Older Glass Mountain lavas exhibit larger (~1‰) variability of $\delta^{18}O$(quartz). The youngest domes of Glass Mountain are similar to BT in $\delta^{18}O$(quartz) values and reflect convective homogenization during formation of BT magma chamber surrounded by extremely heterogeneous country rocks (ranging from 2 to +29‰). Oxygen isotope thermometry of BT confirms a temperature gradient between "Late" (815 °C) and "Early" (715 °C) BT. The $\delta^{18}O$(quartz) values of "Early" and "Late" BT are +8.33 and 8.21‰, consistent with a constant $\delta^{18}O(melt) = 7.8 \pm 0.1$‰ and 100 °C temperature difference. Zircon-melt saturation equilibria gives a similar temperature range. Values of $\delta^{18}O$(quartz) for different stratigraphic units of BT, and in pumice clasts ranging in pre-eruptive depths from 6 to 11 km (based on melt inclusions), and document vertical and lateral homogeneity of $\delta^{18}O$(melt). Worldwide, five other large-volume rhyolites, Lava Creek, Lower Bandelier, Fish Canyon, Cerro Galan, and Toba, exhibit equal $\delta^{18}O$(melt) values of earlier and later erupted portions in each of the these climactic caldera-forming eruptions. We interpret the large-scale $\delta^{18}O$ homogeneity of BT and other large magma chambers as evidence of their longevity ($> 10^5$ years) and convection. However, remaining isotopic zoning in some quartz phenocrysts, trace element gradients in feldspars, and quartz and zircon crystal size distributions are more consistent with far shorter timescales (10^2–10^4 years). We propose a sidewall-crystallization model that promotes convective homogenization, roofward accumulation of more evolved and stagnant, volatile-rich liquid, and develops compositional and temperature gradients in pre-climactic magma chamber. Crystal + melt + gas bubbles mush near chamber walls of variable $\delta^{18}O$ gets periodically remobilized in response to chamber refill by new hotter magmas. One such episode of chamber refill by high-Ti, Sr, Ba, Zr, and volatile-richer magma happened 10^3–10^4 years prior to the 0.76-Ma caldera collapse that caused magma mixing at the base, mush thawing near the roof and walls, and downward settling of phenocrysts into this hybrid melt.

Electronic supplementary material to this paper can be obtained by using the Springer Link server located at http://dx.doi.org/10.1007/s00410-002-0371-8

I.N. Bindeman (✉) · J.W. Valley
Department of Geology and Geophysics,
University of Wisconsin, 1215W. Dayton St.,
Madison, WI 53706, USA
E-mail: inbindem@geology.wisc.edu
Tel.: +1-608-2627118

Editorial responsibility: T.L. Grove

Introduction

The nature, longevity, and dynamics of large silicic magma chambers and granitic batholiths are subjects of considerable controversy. Fluid-mechanics and heat-conduction arguments suggest rapid ($Ra > 10^6$) convection, heat loss and assimilation of country rocks (e.g., Turner and Campbell 1986; Sparks et al. 1990), whereas radiogenic isotopes suggest prolonged residence time, and possibly basalt-fed heating and slow near-conductive cooling (e.g., Halliday et al. 1989; Mahood 1990). Natural evidence, experiments with model fluids and numerical simulations, suggest a variety of often tran-

sient mechanisms by which large silicic magmas are generated, stored, and develop compositional zoning. Points of discussion include the structure of changing convection regimes, the interplay of compositional and thermal effects on density and viscosity, the role of effervescence and crystallization, and the role of boundary vs. internal differentiation (McBirney 1985; Turner and Campbell 1986; Spera et al. 1987; Bergantz 1995; De Silva and Wolff 1995; Dobran 2001). These studies of large silicic magma chambers are pertinent to volcanic hazards, timescales of crustal differentiation, and other fundamental volcanological issues.

Oxygen isotopes provide important new insight into this discussion because oxygen is the main constituent of igneous rocks (50%) and its isotope ratio is not time dependent. Furthermore, oxygen isotopes provide constraints ($\pm 0.1‰$) on the melting source, assimilation and mixing, and reflect temperature variations and the degree of homogeneity of magma bodies. The lateral and vertical variations of $\delta^{18}O$ in silicic magma chambers can be best constrained by studying the products of large-scale caldera-forming eruptions with deep eruptive draw-down of the magma chamber (e.g., Lipman 1984). These processes are harder to investigate in granitic batholiths, where slow plutonic cooling, and other time-integrated epimagmatic and secondary processes, often variably alter $\delta^{18}O$ values of constituent minerals. Primary $\delta^{18}O$ values from the magmatic stage are often difficult to infer for granites, but may be quenched for volcanic rocks. The study of refractory phenocrysts from voluminous ash-flow units offers a unique opportunity to measure magmatic $\delta^{18}O$ values from a cross section of the pre-eruptive magma chamber.

This paper presents an oxygen isotope study of the large (>650 km^3) magma chamber of Bishop Tuff (BT), arguably the best-studied rhyolitic system in the world (Fig. 1, Table 1, Appendix 2). Bishop Tuff provides a series of "snapshots" throughout the batholith-scale magma chamber given the large volume of the erupted material (650 km^3), depth of eruptive draw-down (4–5 km in magnitude, Wallace et al. 1999), and its inferred long-lived nature (3×10^5–10^6 years, Halliday et al. 1989; Bogaard and Schirnick 1995; Christensen and Halliday 1996; Davies and Halliday 1998). Hildreth (1979) described the BT as a classic example of a zoned magma chamber with relatively small gradients of major elements, a 70 °C gradient in temperature, more than twofold variations in trace elements, and variable crystal content (5–25 vol%). Fall deposits of nearly aphyric, allanite-bearing, pyroxene free, high-silica rhyolitic pumice with a low Fe–Ti oxide temperature of ~720 °C was considered to represent the earliest and lowest temperature magma from the top of the magma chamber, whereas a later series of crystal-richer, pyroxene-bearing rhyolitic ignimbrite sheets with progressively increasing temperature (to 790 °C) was interpreted to represent more deeply tapped, hotter portions of the chamber. Subsequent studies have demonstrated that the BT magma body exhibited an upward increase in the concentration of water and volatile elements (B, F, Cl; Dunbar and Hervig 1992; Wallace et al. 1999; Anderson et al. 2000) and an increase in $^{87}Sr/^{86}Sr_i$ ratios (0.706 to 0.709, Halliday et al. 1984). The roofward increase in $^{87}Sr/^{86}Sr_i$ correlates with decrease in Sr and increase in Rb concentration, and is the basis for internal isochrons

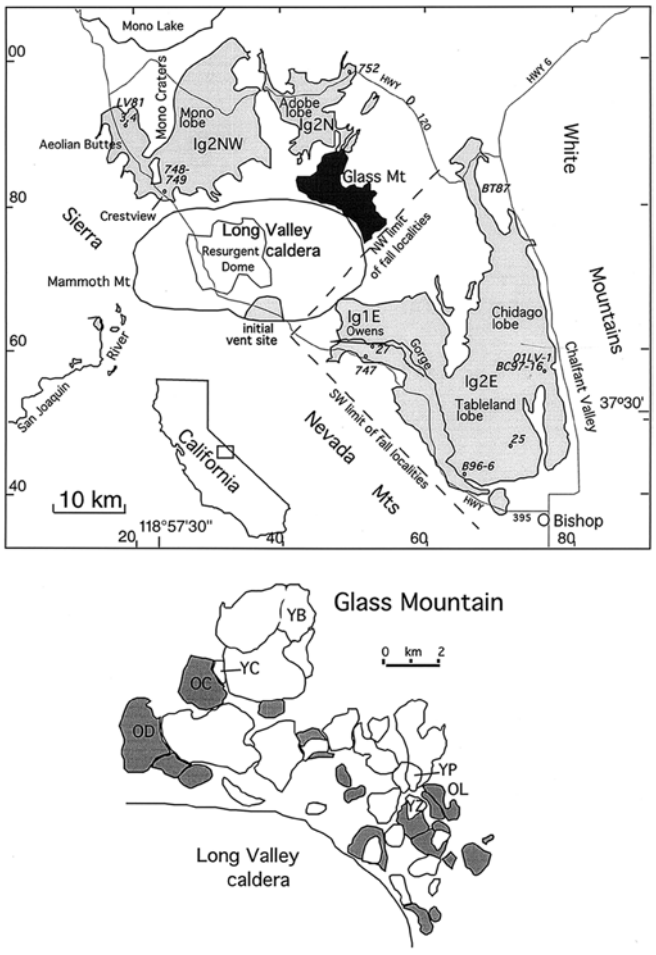

Fig. 1. Map of Long Valley Caldera and vicinity (*top*) and enlargement of Glass Mountain area (*bottom*). Lobe names are from Hildreth (1979), new names of ignimbrite and fall units (Ig, F, Table 1) are from Wilson and Hildreth (1997); sample localities and abbreviated numbers (99LV-) are shown for Bishop Tuff and analyses are given in Table 1. *Numbers 20, 40, 60, 80* next to *tic marks on the frame* are UTM coordinates. At Glass Mountain, Older (2.1–1.2 Ma) domes are *dark*, Younger (1.2–0.79 Ma) domes are *white*. Long Valley caldera is surrounded by Paleozoic and Mesozoic metavolcanic and metasedimentary rocks, as well as Mesozoic Sierra Nevada granitoids, and is superimposed on the major Sierran fault (Bailey 1989). Many of these country rocks are present as clastic inclusions throughout the BT and were used to infer the sequence of caldera ring fracture propagation during the 0.76-Ma caldera-forming eruption (Hildreth and Mahood 1986; Wilson and Hildreth 1997). Sierra Nevada granitoids in the vicinity of Long Valley have $\delta^{18}O(WR)$ values of +8 to +9‰ (Masi et al. 1981); metasedimentary rocks range from +8 to +29‰ in some metacarbonates of Mt. Morrison roof pendant (Smith and Suemnicht 1991; Lackey and Valley 1999) to 2‰ in hydrothermally altered volcanic rocks below BT exposed at depths down to 2 km in drill holes (McConnell et al. 1997). Plutonic and metasedimentary rocks also show a wide range in Sr isotope compositions (0.706–0.725), usually exceeding that of BT (Goff et al. 1991)

Table 1. Oxygen isotope analyses of phenocrysts from Bishop Tuff, Glass Mt, and post-caldera volcanics. Unit names and locations are from Wilson and Hildreth (1997), and Bailey (1989). *Roman numerals* denote a pumice clast number, *Arabic numerals* denote a crystal number; *I-3.4* clast 1 and phenocrysts of 3.4 mg; Phenocryst weight in mg is designated: *bg* big >5 mg; *md* medium 2–5 mg; *sm* small <2 mg; where no pumice clast number is given, quartz was extracted from bulk sample either because strong welding obliterated individual pumice clasts, or because of small pumice size. Qz-1 individual phenocryst of quartz; *Cpx* and *Opx* are clino- and orthopyroxenes; *Zrc* and *Mt* are zircon and magnetite; *Obs* is obsidian (glass). Temperatures are calculated based on $\Delta^{18}O$(Qz–Mt) using Chiba et al. (1989) calibration

No.	Sample[a]	$\delta^{18}O‰$
Glass Mountain		
1	99LV-753	YP. 0.98 Ma
	Qz, bulk	8.56
	Qz, bulk	8.75
2	99LV-759	OD. 1.35 Ma
	Qz, bulk	8.69
	Qz, bulk	8.62
3	99LV-755	OC. 1.92 Ma
	Qz, 3sm	9.15
	Qz, 3sm	9.01
4	99LV-757	YC. 1.35 Ma
	Qz, 3sm	8.73
	Qz, 3sm	8.68
5	OOLV-5	OL. 1.6 Ma
	Qz-1, sm	8.61
	Qz-1, sm	8.64
6	OOLV-7	OL. 1.6 Ma
	Qz-1, md	8.72
7	OOLV-4	YB. 0.98 Ma
	Qz, bulk	8.46
	Qz-1, sm	8.20
	Obs	8.11
8	OOLV-6	YZ. 0.82 Ma
	Qz-1, sm	8.36
	Qz-1, sm	8.19
	Qz-1, sm	8.43
	Obs	8.29
Bishop Tuff, 0.76 Ma Fall units		
9	B96-6-1	F1
	Qz-1, bg	8.59
	Qz-1	8.31
	Qz-1	8.23
	Mt, bulk	2.42
	Mt, bulk	2.46
	T, °C	756
10	B96-6-4	F4
	Qz-1, bg	8.35
	Qz-1, md	8.68
	Qz-1, md	8.50
	Mt, bulk	2.05
	T, °C	714
11	B96-6-5	F5
	Qz-1, bg	8.33
	Qz-1, bg	8.36
	Mt, bulk	2.18
	T, °C	737
12	B96-6-6A	F6
	Qz-1, I-9	8.38
	Qz-1, I-9	8.31
	Qz-1, I-md	8.69
	Mt, bulk	2.22
	T, °C	731
13	BT87-2	F5
	Qz-1, I-6.2	8.47
	Qz-1, I-6.2	8.47
	Qz-1, I-md	8.64
	Mt, bulk	2.36
	Mt, bulk	2.51
	T, °C	743
14	BT87-3	F6
	Qz-1, I-bg	8.47
	Qz-1, I-md	8.48
	Mt, bulk	2.75
	T, °C	775
15	BT87-8B	F7
	Qz-1	10.57
16	BC97-16	F7
	Qz-1, I-6.7	8.15
	Qz-1, I-2.3	8.27
	Qz-1, I-1.6	8.22
	Qz-1, I-md	8.09
	Qz-1, I-sm	8.14
	Qz-1, I-bg	8.22
	Qz-1, I-2.6	8.35
	Qz-1, I-5.2	8.21 ± 0.09
	Qz-1, I-bg	7.72
	Qz-1, I-md	8.44
	Qz-1, I-md	8.35
	Qz-1, I-10sm	8.19
	Mt, bulk	2.22
	T, °C	754
17	01LV-1	F9
	Qz-1, I-2.1	8.54
	Qz-1, I-md	8.49
	Mt, bulk	2.30
	Mt, bulk	2.34
	T, °C	735
Bishop Tuff, ignimbrites		
18	99LV-747	Ig1Ea
	Qz-1, I-1	8.16
	Qz-1, I-2	8.33
	Qz-1, III-1	8.28
	Mt, bulk	1.99
	Mt, bulk	2.1
	T, °C	734
19	OOLV-27	Ig1Ea
	Qz-1	8.32
	Qz-1	8.25
	Qz-1	8.23
	Mt, bulk	1.81
	Zrc, bulk	5.44
	Zrc, bulk	5.71
	Zrc, bulk	5.63
	T, °C	714
20	OOLV-25	Ig2E
	Qz-1	8.06
	Qz-1, I-bg	8.40
	Qz-1, I-sm	8.43
	Mt, bulk	2.49
	Mt, bulk	2.43
	Cpx, bulk	5.74
	Cpx, bulk	5.72
	T, °C	765
	Cpx-Mt, T, °C	758
21	LV81-18a	Ig2NWb
	Qz-1, I-12.3	8.30
	Qz-1, I-bg	8.15
	Qz-1, I-3.4	7.94 ± 0.10
	Qz-1, I-5.2	8.08 ± 0.20
	Qz-1, I-7.5	8.18 ± 0.27
	Qz-1, I-5.8	7.95
	Qz-1, I-8.2	7.84
	Qz-1, I-8.3	8.14
	Qz-1, I-1.2	8.11
	Qz-1, I-bg	8.14

Table 1. (Contd.)

No.	Sample[a]	$\delta^{18}O‰$
	Qz-1, I-bg	8.14
	Qz-1, I-14.1	8.15 (rim)
	Qz-1, I-13.3	8.39 (rim)
	Qz-CR, I-21.4	8.22 (core)
	Qz-CR, I-21.4	8.09 (core)
	Qz-CR, I-21.4	7.88 (core)
	Qz-CR, I-21.4	8.13 (core)
	Qz-CR, I-21.4	8.3 (rim. outer 20%)
	Qz-CR, I-21.4	8.37 (rim)
	Qz-CR, I-21.4	8.36 (rim)
	Qz-CR, I-21.4	8.18 (rim. outer 10%)
	Qz-CR. I-21.4	8.07 (rim, outer 10%)
	Mt, bulk	2.72
	Mt, bulk	2.85
	Cpx, bulk	5.79
	T, °C	819
	Cpx-Mt, T, °C	814
22	00LV-3	Ig2NWb
	Qz-1, I-sm	8.04
	Qz-1, I-md	8.20
	Qz-1, I-sm	8.19
	Qz-1, I-bg	8.20(core)
	Mt, bulk	2.29
	Mt, bulk	2.31
	Opx, bulk	5.83
	Opx, bulk	6.03
	Zrc, bulk	5.83
	Zrc, bulk	5.82
	T, °C	763
23	01LV-4	Ig2NWb.enclave
	Qz-1, I-sm	8.35
	Qz-1, I-7.1	8.47
	Qz-1, I-md	8.46
	Mt, bulk	2.87
	Mt, bulk	2.74
	T, °C	785
24	99LV-748	Ig2NWa
	Qz-1, I-1	8.23
	Qz-1, I-3	8.19
	Qz-1, I-4	8.12
	Qz-1, II-2	8.32
	Qz-1, II-3	8.31
	Qz-1, III-1	8.34
	Qz-1, III-2	8.19
	Mt, bulk	3.03
	Mt, bulk	2.86
	Zrc, bulk	5.93
	Zrc, bulk	5.95
	T, °C	817
25	99LV-749	Ig2NWa
	Qz-1, I-1	8.29
	Qz-1, I-2	8.26
	Qz-1, I-3	8.38
	Qz-1, II-4	8.17
	Qz-1, III-1	8.13
	Qz-1, III-3	8.59
	Qz-1, III-2	8.43
	Mt, bulk	2.48
	Mt, bulk	2.73
	T, °C	776
26	99LV-751	Ig2Na
	Qz-1, I-1	8.32
	Qz-1, I-2	8.30
	Qz-1, I-3	8.31
	Qz-1, II-1	8.17
	Qz-1, II-3	8.29
	Qz-1, III-2	8.08
	Qz-1, III-3	8.31
	Mt, bulk	2.13
	Mt, bulk	2.20
	Zrc, bulk	5.85
	Zrc, bulk	6.12
	Zrc, bulk	5.86
	T, °C	743
27	99LV-752	Ig2Na
	Qz-1, I-2	8.26
	Qz-1, III-1	8.44
	Qz-1, II-4	8.43
	Mt, bulk	2.39
	Mt, bulk	2.43
	T, °C	754
Post-calderas		
28	00LV-28	0.65 Ma
	Obs	8.11
29	00LV-18	0.65 Ma
	Obs	8.09
	Basaltic enclave	
	WR	6.25
	Plag	6.56
	Cpx	5.31
	An_{70}–Cpx T, °C	886
30	OOLV-23	Qmr2. 0.36–0.33 Ma
	Qz-1	8.07
	Qz-1	8.36
31	00LV-24	Qmrh, 0.33–0.29 Ma
	Obs	8.14
32	OOLV-12	Qmr3, 0.16–0.12 Ma
	Qz-1	8.15
	Qz, bulk	8.19
33	OOLV-13	Qri, 0.10 Ma
	Qz, bulk	8.36
34	00LV-15	Qp, 0.04 Ma
	Obs	8.05

[a]GPS grid and sample location. *Glass Mountain*: (*1*) 351461, 4182251, McGee Cyn. Rd to Sawmill Meadows; (*2*) 340128, 4183691, 1 mile ESE McLaughling Spring; (*3*) 343030, 4185427, Wet Meadows; (*4*) 343538, 4185905, slope of Wet Meadows; (*5*) 351476, 4180752, top of ridge; (*6*) 351377, 4180891, N slope of dome; (*7*) 346912, 4188575,W slope of dome; (*8*) 350960, 4180521, N slope of dome. *Bishop Tuff*: (*9*) Pleasant Valley Dam, Tableland, 1 inch above base; (*10*) same, 11 inches above base; (*11*) same, from 2 ft to 5 ft 6″ above base; (*12*) same, 1 inch below top of F6; (*13*) Blind Spring Hill, Gorges, loc. 104 of Hildreth (1979), 3 ft 2″ above base; (14) same, 5ft 10‘‘ above base; (*15*) same; (*16*) Chalfant quarry, Chidago; (*17*) same ; (*18*) 353632, 4180521, Gorges, pumice roadcut, loc 19 of Wilson and Hildreth (1997), rt 395; (*19*) 361635, 4151303, Gorges, Owens River Gorge; (*20*) 374728, 4142975, Tableland, Tableland road; (*21*) Aeolian Buttes, Adobe, top of hill; (*22*) same, 317565, 4192479; (*23*) same; (*24*) 323943, 4181516, Mono, Crest View, roadcut loc 208 of Wilson and Hildreth (1997), E side of rt 395, 33 m above rd. level; (*25*) same, 25 m above rd. level; (*26*) 349663, 4198176, Adobe, N side rt 120, loc 135; (*27*) same. *Post Caldera*: (*28*) 329069, 4174380, N of Smokey Bear Flats; (*29*) 333190, 4171793, top of hill W of Little Antelope Valley; (*30*) 340365, 4170695, SE moat; (*31*) 339052, 4165598, Hot Creek Dome, NE; (*32*) 322714, 4174095, summi summit of Deer Mt; (*33*) 322866, 4175547, Deadman Creek Dome, SE; (*34*) 328353, 4177647, Lookout Mt., top

because of in-situ fractionation and aging (Halliday et al. 1989; Davies and Halliday 1998).

Despite significant progress in understanding the Long Valley magma system with respect to radiogenic isotopes, trace elements, and volatiles, oxygen isotope studies of magmatic values for BT and Glass Mountain (GM) are limited (e.g., Halliday et al. 1984). Most other

oxygen isotope studies concentrated on hydrothermally altered rocks from the surface and in bore holes (Smith and Suemnicht 1991; McConnell et al. 1997; Holt and Taylor 1998). In this work, we analyzed individual phenocrysts in single pumice clasts from extra-caldera BT localities and concentrated on the primary pre-eruptive oxygen isotopic composition throughout the magma chamber. With the ability to analyze sample sizes smaller than typical igneous phenocrysts (1–2 mg), and refractory minerals zircon, magnetite, and pyroxene, we describe and interpret subtle variations in $\delta^{18}O$ in the BT magma chamber on the order of 0.1–0.2‰, assess isotopic equilibria between individual phenocrysts, and estimate temperatures. Additionally, this paper addresses longevity of magma system under Long Valley caldera, considers temporal $\delta^{18}O$ trends through the eruptive sequence GM to BT to post-BT, presents zircon- and quartz-crystal size distributions, and interprets new isotopic data in context of other published results for melt inclusions and radiogenic isotopes.

Sample collection and analytical techniques

Samples

In this work, we follow the stratigraphic scheme of Wilson and Hildreth (1997), and refer to "Early" BT as representing fall deposits (F1–F7) and the Ig1 ignimbrite sheet; and "Late" BT as representing Ig2E, Ig2NWa,b and Ig2 N ignimbrite sheets. Sample collection of BT was tied to the exact localities of Wilson and Hildreth (1997) using the global positioning system, and field photographs from their paper. Sampling of GM and post-caldera lavas was done using the geologic maps of Bailey (1989) and Metz and Bailey (1993). Additionally, we analyzed quartz from pumice clasts of BT (Table 1) that were studied earlier by F. Lu, Fred Anderson, and Paul Wallace. These clasts are ash-fall samples with the lowest pumice density (0.71 g/cm^3, BT87-2, and 0.26 g/cm^3 BT87-3), the shallowest pre-eruptive depth (6 km, BC97-16), and the deepest pre-eruptive depth (~11 km, LV81-18a) based on estimation of CO_2 and H_2O concentrations in melt inclusions and assuming fluid saturation (1.45–2.8 kb, Wallace et al. 1999). Also, a sample of coeval dark Ba- and Zr-rich crystal-poor low-silica rhyolitic enclave from the latest erupted BT (01LV-4) was analyzed (see Table 2 for selected XRF whole-rock analyses of pumice clasts).

Mineral separation

Quartz phenocrysts were extracted from individual pumice clasts (ranging in weight from several grams to 500 g) under a binocular microscope, and the weight and size of each quartz phenocryst was recorded. Quartz was purified with cold fluoroboric (HBF_4) acid for 10–20 min, or HF for up to 5 min in order to remove any attached glass and hourglass melt inclusions. A variable amount of internal glass inclusions, typically <2 vol%, was unavoidably present. Phenocrysts were checked for the presence of such melt inclusions to ensure that none of the analyzed crystals were secondary (secondary quartz is rare and is characterized by single-terminated pyramidal shape and is free of melt inclusions). Because glassy melt inclusions are sealed within the quartz phenocrysts, they are fresh and unaltered. Thus, their contribution to the uncertainty in $\delta^{18}O$ is negligible (ca. 0.01–0.02‰). Three to 16 individual quartz phenocrysts were typically extracted and analyzed in each sample. Several large (>5 mg) quartz phenocrysts were studied for core-to-rim zoning in $\delta^{18}O$ by cross sectioning and microdrilling. Magnetite crystals were separated from the crushed pumice with a Nd ceramic magnet. Five to ten optically unaltered and shiny octahedral crystals (0.1–0.3 mg each) were picked for each analysis. Green clinopyroxene was picked from crushed rock and analyzed in bulk. Zircons were extracted from four large pumice clasts (200–250 g) by HF dissolution and analyzed in bulk. Fresh, densely welded obsidian samples were chosen for analysis in selected GM, late BT, and post-caldera lavas.

Stable isotope analyses

The University of Wisconsin CO_2-laser fluorination/mass-spectrometer system allowed us to obtain accurate and precise oxygen isotope ratios for minerals and glass samples that were typically 1–2 mg, yielding 10–30 μmol of CO_2 (e.g., Valley et al. 1995). Yields were 90–102%, and there is no correlation between yield, sample size, and $\delta^{18}O$. We used bromine pentafluoride (BrF_5) as a reagent. Minerals were pre-treated with 5 torr of BrF_5 overnight to remove any surface or water contamination. For obsidian, no pretreatment was performed and an air-lock chamber was used (Spicuzza et al. 1998a). Analyses of quartz used a rapid heating technique (Spicuzza et al. 1998b) with precision better than ± 0.1‰. Duplicated analyses of magnetite were typically within ± 0.06‰. From four to seven aliquots of UWG-2 garnet standard were measured at the beginning and end of each day of analyses. The average reproducibility of 65 analyses of UWG-2 was 5.71 ± 0.10‰ (1 SD, 1 SE = ± 0.01‰). Thirty analyses of NBS-28 quartz yielded a value of 9.44 ± 0.08‰ (1 SD, 1 SE = ± 0.02‰, relative to V-SMOW, Table A, Supplementary Electronic material). A correction in the range of $+0.3$‰ to -0.05‰ ($+0.15$ to 0‰ for most days) was applied to account for day-to-day variations based on values of five to seven UWG-2 garnets measured during each analytical session as recommended by Valley et al. (1995). Thus, the overall analytical uncertainty on single measurements was better than ± 0.10‰, and possibly better than ± 0.08‰ (1 SD).

Oxygen isotope analyses of populations of individual quartz phenocrysts in pumice clasts were compared using four statistical parameters: mean, standard deviation, standard error, and *t*-test (Davis 1973). The mean and

Table 2. Major and trace element composition of individual pumice clasts of major ignimbrite units of Bishop Tuff; all analyses are by XRF (XRAL Labs, Ontario, Canada). Zircon quenching (=eruption) and saturation temperatures was calculated using Watson and Harrison (1983), see text for discussion

Sample	99LV-751	99LV-751a	99LV-748	99LV-748a	00LV-3	01LV-4	00LV-25	00LV-27
Unit	Ig2Na	Ig2Na	Ig2NWa	Ig2NWa	Ig2NWb	Ig2NWb	Ig2E	Ig1Ea
Clast	Clast V	Clast V	Clast I	Clast I	Clast I	Enclave	Clast I	Welded tuff
wt%								
SiO_2	75.9	75.8	73.2	73.3	73.1	70.2	74.3	77.9
TiO_2	0.125	0.125	0.168	1.165	0.159	0.269	0.129	0.074
Al_2O_3	11.9	11.9	13.3	13.3	12	12.4	12.7	12
Fe_2O_3	1.15	1.14	1.36	1.3	1.19	2.23	1.19	1.02
MnO	0.02	0.02	0.02	0.02	0.04	0.06	0.03	0.03
MgO	0.08	0.08	0.17	0.17	0.38	0.8	0.16	0.01
CaO	0.65	0.65	0.74	0.14	1.25	1.29	0.84	0.56
Na_2O	3.26	3.24	2.96	2.95	3.19	2.15	2.94	3.86
K_2O	5.02	5.04	5.37	5.34	5.29	4.38	5.74	4.53
P_2O_3	0.02	0.02	0.02	0.01	0.09	0.13	0.04	0.02
Sum	100.2	100.1	100.3	100.3	100.4	100.3	100.3	100.2
LOI	2.05	2.05	2.8	2.9	3.59	6.15	2.05	0.15
ppm								
Rb	114	115	118	114	103	101	144	160
Sr	43	42	64	64	106	126	48	13
Y	20	20	18	17	17	22	25	29
Zr	119	117	140	140	138	158	121	89
Nb	16	15	14	14	13	12	20	25
Ba	217	216	359	356	445	904	236	98
Phenocrysts (%)	13	13	15	15	27	5–10	10–15	10
Zircon (ppm)	31	31	33	33	54			24
T saturation (°C)	763	763	784	784	762	801	763	737
T quench (°C)	761	761	776	776	767			735
T, Δ^{18}(Qz–Mt), °C	743	743	817	817	763	785	765	714

standard error describe how well the average value is known, standard deviation is useful to predict reproducibility of additional analyses to a sample population, whereas the *t*-test determines if the mean values of two different populations are statistically different within a certain confidence level. The use of these parameters assumes that analyses are distributed normally, and we demonstrate below that normal distributions are evident on histograms.

Results

δ^{18}O change during 2 million years of magmatic evolution

Figure 2 presents analyses of quartz and glass arranged vs. radiometric or inferred stratigraphic age for the 2-million-year-long volcanic evolution: Glass Mountain (pre-caldera), BT(caldera-forming ignimbrite and ash), and post-caldera, intra-caldera lavas.

Glass Mountain

Most GM lavas contain very few or no quartz phenocrysts. Quartz phenocrysts were analyzed individually and in bulk (where size did not allow individual analyses) in seven domes of Glass Mountain (GM), three in older lavas, and four in younger lavas (Table 1, Fig. 2). Older GM have 0.2–0.8‰ higher δ^{18}O(Qz) values then BT, and exhibit ~1‰ heterogeneity among lavas. The δ^{18}O(Qz) values of the youngest units (YB and YZ), which erupted shortly before the climactic 0.76-Ma eruption of BT, are 0.4‰ lower than other younger GM lavas and are identical in δ^{18}O(Qz) to the BT. These observations closely match trace element concentrations and ratios (e.g., REE, Rb/Sr, Sm/Nd), which suggest (1) a larger chemical variability, and less-differentiated nature of older GM lavas, and (2) a close trace element similarity and highly differentiated nature of young GM lavas and BT (Metz and Mahood 1991; Metz and Bailey 1993).

Bishop Tuff

Thirty-four individual quartz phenocrysts in fall units and Ig1E (Early, cold BT) give $\delta^{18}O(Qz) = 8.33 \pm 0.03$‰ ($\pm 1$ SE, ± 0.17‰ 1 SD) mean value. Forty-eight quartz phenocrysts (63 analyses) of Ig2 (Late, hot BT) units give $\delta^{18}O(Qz) = 8.21 \pm 0.03$‰ ($\pm 1$ SE, ± 0.14‰ 1 SD) mean value defining a subtle 0.12‰ difference between mean values (Fig. 3A). All together, among 82 individual quartz phenocrysts analyzed in BT, we found no low-δ^{18}O values, which would indicate involvement of a low-δ^{18}O rock or magma. Only one cloudy and anhedral high-δ^{18}O quartz xenocryst ($\delta^{18}O = 10.57$‰, sample BT87-8b, Table 1) is present in the F7 fall deposit. Values of δ^{18}O(Qz) and δ^{18}O(Mt) in latest erupted Ba- and Zr-rich, crystal-poor inclusion (sample 01LV-04) are 0.2‰ higher than that in dominant crystal-rich (ca. 25 vol%) rhyolitic pumice clasts of Latest BT.

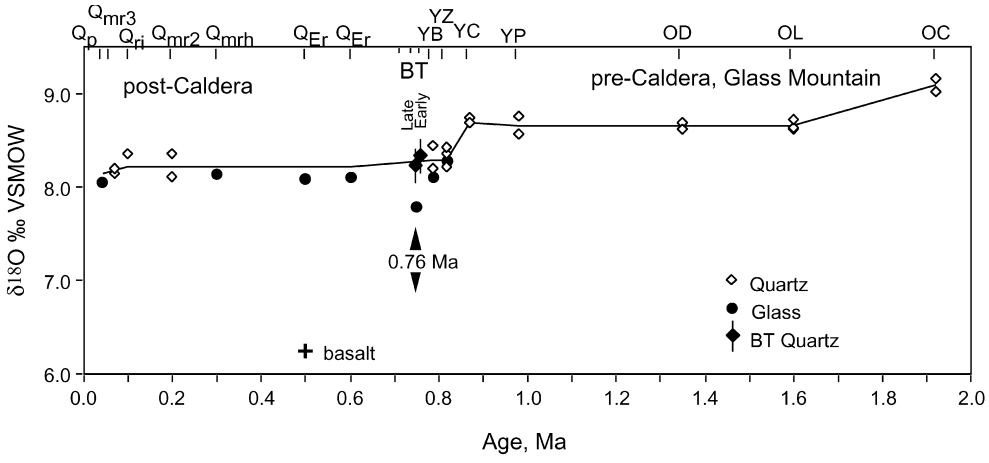

Fig. 2. Evolution of $\delta^{18}O$ values in Glass Mountain-Bishop Tuff magma system. Unit names are from Table 1. Notice larger range and slightly higher $\delta^{18}O$(quartz) values in older Glass Mountain lavas, similar $\delta^{18}O$ values of 2 youngest Glass Mountain lavas and Bishop Tuff, and an overall similarity of $\delta^{18}O$ values in post-caldera lavas. *Solid line* represents the trend for melt in equilibrium with quartz (see text)

We compiled published $\delta^{18}O$ analyses of bulk quartz by McConnell et al. (1997), Smith and Suemnicht (1991), and Holt and Taylor (1998). McConnell et al. (1997) sampled phenocrysts and glass in drill holes through the 2 km-thick sequence of intra-caldera Bishop Tuff, and post-caldera Early rhyolite. We assume that the sequence of BT in drill holes roughly corresponds to its stratigraphy of deposition from various parts of the migrating vent during caldera-forming eruption. The sequence, therefore, correlates to its inverse position in the magma chamber, and each drill hole provides another "cross section" through the upper part of the magma chamber, as does the stratigraphy of Wilson and Hildreth (1997), employed in this study. While whole-rock samples have suffered variable degrees of hydrothermal alteration at depth in drill holes (McConnell et al. 1997), and on the surface (Smith and Suemnicht 1991; Holt and Taylor 1998), quartz phenocrysts are least affected, and the $\delta^{18}O$(Qz) are in overall agreement with $\delta^{18}O$ ranges of the results above.

Post-caldera lavas

Post-caldera, intra-caldera lavas tend to be quartz-poor and exhibit a high degree of hydrothermal alteration in and around the resurgent dome. Unaltered samples do not show changes in $\delta^{18}O$ of quartz and glass as compared with BT (Fig. 2), despite significant changes in mineralogy, and major and trace element composition (Bailey et al. 1976; Heumann and Davies 1997; Heumann 1999). The $\delta^{18}O$(Cpx) and $\delta^{18}O$(Pl) values of a 5-cm-diameter basaltic enclave in 650 ka Early rhyolite suggest $\delta^{18}O$(magma) values of 6.2‰, close to the typical MORB value of 5.8 ± 0.2‰.

$\delta^{18}O$ vs. $^{87}Sr/^{86}Sr$, $^{206}Pb/^{204}Pb$, and ϵNd

Oxygen isotope analyses of the present study complement radiogenic isotope analyses performed on the same units over the past 20 years. A subtle 1‰ temporal decrease in $\delta^{18}O$(quartz) values in silicic lavas from the earliest (2.0 Ma) Glass Mountain lavas toward post-caldera volcanics (Fig. 2) correlates with a decrease in $^{87}Sr/^{86}Sr_i$ (corrected for K–Ar eruption age), increase in ϵ_{Nd}, and an increase in $^{206}Pb/^{204}Pb_i$ (Fig. 4). A significant range of ϵ_{Nd} in Glass Mountain lavas –1 to –4) negatively correlates with $\delta^{18}O$(Qz), suggesting mixing and progressive homogenization of mantle-derived (less-negative ϵ_{Nd} and lower $\delta^{18}O$) and upper-crustal-derived (more negative ϵ_{Nd}, and higher $\delta^{18}O$) melts. Based on the "neodymium crustal index" (DePaolo et al. 1992), BT contains 25% of upper crust, whereas Early Glass Mountain lavas may contain up to 40%, assuming Nd and ϵ_{Nd} end member compositions as in Knesel and Davidson (1997). High $^{87}Sr/^{86}Sr_i$ values, and significant range of initial $^{87}Sr/^{86}Sr_i$ values of GM and BT, are attributed to extreme variations in Rb/Sr ratio as a function of variable differentiation and in-situ aging in the long-lived magma chamber (e.g., Halliday et al. 1989). There is a very subtle positive correlation of $^{87}Sr/^{86}Sr_i$ with $\delta^{18}O$ (Fig. 4). Lead isotopes are most variable in post-caldera lavas and are generally higher (at lower $\delta^{18}O$) than GM. The temporal lowering of $\delta^{18}O$ (Fig. 2) supports the model of progressive addition, fractionation, and mixing of a normal-$\delta^{18}O$ magma (5.8–6.0‰), a fractionate of a mantle-derived basalt, into the base of the silicic magma system (e.g., Christensen and DePaolo 1993; Heumann and Davies 1997; Heumann 1999). However, the lack of a single trend in correlation between Sr, Nd, Pb, and O isotopes suggests that both the source region (lower to middle crust), and assimilants in the upper crust are diverse. A multiple end member model with sources and country rocks of variable isotopic composition should be considered.

Oxygen isotope cross section through the Bishop Tuff magma body

$\delta^{18}O$ values of quartz in single pumice clasts of Bishop Tuff

Table 1 and Fig. 3 compare the $\delta^{18}O$ values of individual quartz phenocrysts of BT. The $\delta^{18}O$(Qz) values from two pumice clasts, one from Early (F7, sample BC97-16) and

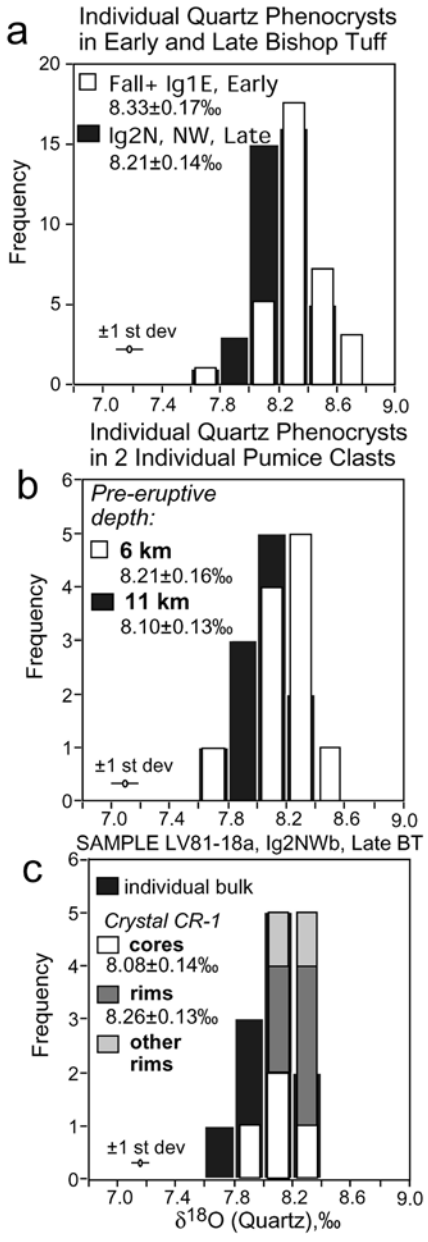

Fig. 3A–C. Values of $\delta^{18}O$ for individual quartz phenocrysts in single pumice clasts from BT, see Table 1 for analyses. The range of $\delta^{18}O$ in Bishop Tuff quartz values reflects natural dispersion around the mean (shown as ± 1 SD), and not an analytical error, see text for discussion. Application of a *t*-test suggests that subtle 0.12‰ differences between different quartz populations of >11 analyses each are significant within 97–99% confidence level. **A** Individual quartz phenocryst analyses in Early and Late Bishop Tuff. **B** Individual quartz phenocrysts in two pumice clasts: samples LV81-18a (Ig2NWb, Late) and BC97-16 (F7, Early). These two clasts represent the deepest and the shallowest BT according to melt inclusion studies (Wallace et al. 1999). **C** Cores and rims of quartz phenocrysts in pumice clast LV81-18a

one from Late BT(Ig2NWb, sample LV81-18a) show almost identical near-normal distributions (Fig. 3B). The average $\delta^{18}O$(Qz) value in BC97-16 is 8.21 ± 0.05 (1 SE, 12 crystals, 13 analyses, 1 SD = 0.16‰) vs. 8.10 ± 0.04 (± 1 SE, 14 crystals, 25 analyses, 1 SE = 0.13‰) in LV81-18a. These two clasts represent magma batches with inferred pre-eruptive depths of 6 and 11 km, respectively, based on melt-inclusion studies (Wallace et al. 1999). The range of $\delta^{18}O$(Qz) in these two clasts overlaps with $\delta^{18}O$(Qz) values for Early and Late BT (Fig. 3A). These values show a total range of 0.5–0.6‰ that exceeds our analytical uncertainty. We interpret these subtle trends as significant and to reflect natural variations.

We also performed analyses of rims and cores of several large crystals, and analyses of small vs. large crystals in pumice clasts BC97-16 and LV81-18a in order to measure any intracrystalline $\delta^{18}O$ variations. Peppard et al. (2001) reported that all quartz phenocrysts in Ig2NW ignimbrite sheet, and in sample LV81-18a, in particular, are overgrown by a primary magmatic bright-cathodoluminescence (CL) rim that constitutes 10–25% of the external radius (60% volume). These rims contain melt inclusions studied by Wallace et al. (1999) and Anderson et al. (2000), with least-differentiated, high-Ba, Zr compositions. Oxygen isotope analyses of quartz rims (outer 20% of radius, 50% of volume) in the same pumice clast LV81-18a, resulted in 0.15‰ higher $\delta^{18}O$ values than cores (Fig. 3C). One large 2.5-mm-long, 21-mg perfectly faceted crystal in this pumice clast gave a 0.19‰ difference between four analyses of core and five analyses of rims (Table 1, Fig. 3C). This quartz crystal does not exhibit a concentric core-to rim increase in $\delta^{18}O$ because rims on different sides of this crystal are 0.3‰ apart. We found no correlation between the size of individual quartz phenocrysts and $\delta^{18}O$(Qz) in two pumice clasts. We conclude that the 0.5–0.6‰ range reflects random intercrystalline and intracrystalline variation, discussed below, but the normal-distribution of $\delta^{18}O$ values around the mean justifies the use of the mean as the close proxy for calculating $\delta^{18}O$(melt), and $\Delta^{18}O$(Qz–Mt) temperatures below.

Heterogeneous $\delta^{18}O$ values in individual quartz phenocrysts

The 0.5–0.6‰ variability of quartz in a single hand specimen can be explained by quartz alteration by meteoric water during and shortly after the eruption, or as a primary magmatic feature. Heated meteoric fluids may lead to lower $\delta^{18}O$(Qz) values, whereas low-T exchange with such fluids may lead to higher-$\delta^{18}O$(Qz) values. Thus, quartz interaction with meteoric water at high, and then low-T can create a $\delta^{18}O$ range among different quartz phenocrysts, and core-to-rim variations in single phenocryst, which underwent variable degrees of exchange. However, several lines of evidence argue against the possibility of exchange with meteoric water. First, we notice the chemically pristine nature of analyzed pumice, and the presence of unaltered and undevitrified magmatic melt inclusions even in the outermost parts of crystals (Wallace et al. 1999; Anderson et al. 2000; Peppard et al. 2001). Second, an extensive CL study of quartz, with the same pumice clasts by Peppard et al. (2001), found no evidence of post-magmatic alteration

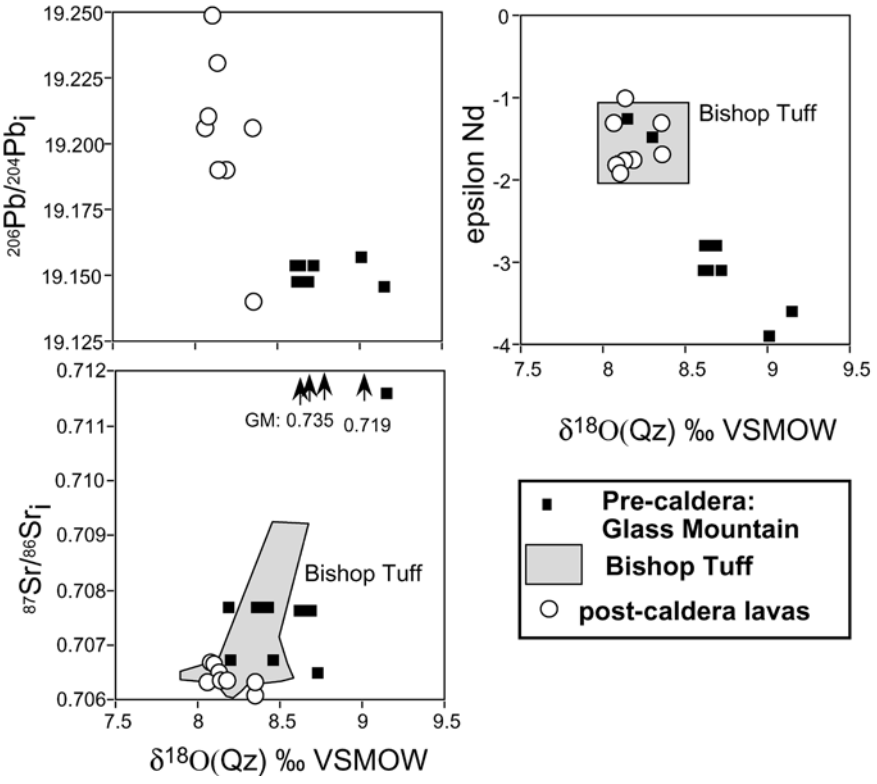

Fig. 4. Correlation between $\delta^{18}O$(Qz) and initial $^{206}Pb/^{204}Pb$, $^{87}Sr/^{86}Sr$, and ϵ_{Nd} of Glass Mountain, Bishop Tuff, and post-caldera rhyolites. Radiogenic isotope analyses for the same units are from Halliday et al. (1989), Davies and Halliday (1998), and Heumann (1999). Sr isotope ratios are given for the K–Ar time of eruption

features such as crack filling, or a secondary rim. Third, is the rapid eruption dynamics, and subsequent cooling, estimated to last minutes and months/years respectively (Wilson and Hildreth 1997). By diffusion at high T (500 °C) for 1 year, quartz would exchange oxygen only in its outer 1 μm (Farver and Yund 1991). Fourth, a simple mass balance calculation suggests that even a 100-μm rim on a 2-mm-diameter crystal constitutes only 9% of crystal's volume, and $\delta^{18}O$(rim) should be $< 7‰$ different from the $\delta^{18}O$(core) to account for $\pm 0.3‰$ shifts in bulk quartz $\delta^{18}O$ values. We conclude that the 0.6‰ range is magmatic in origin and discuss how it was generated and preserved.

Thermometry of the Bishop Tuff magma chamber

Oxygen isotope thermometry

Application of the $\Delta^{18}O$(Qz–Mt) experimental calibration of Chiba et al. (1989) to BT ignimbrite and fall units (Table 1, Fig. 5) shows a 100 °C temperature gradient from early to later erupted rhyolites. Figure 5 compares these results with the Fi–Ti oxide temperatures of Hildreth (1979) (Fig. 5a), and the calculated zircon-melt quench temperatures are shown in Table 2 and Fig. 5b. The Fe–Ti oxide temperatures of Hildreth (1979) used an earlier stratigraphic scheme. When cross correlated with the new eruptive stratigraphy of Wilson and Hildreth (1997) using the same eruptive units (Fig. 5a), there is a reasonable correspondence of oxide and isotope temperature ranges of ca. 70–100 °C. Thick (>100m) and densely welded Ig1 and Ig2 ignimbrite sheets exhibit similar or higher oxygen isotope temperatures than that calculated from rapidly quenched 2–10-cm pumice clasts of fall deposits. This suggests that the calculated temperatures reflect eruptive quench and not post-emplacement cooling conditions.

When the new eruptive stratigraphy of Wilson and Hildreth (1997) is employed, there is a steady ~100 °C increase in temperatures from the earlier-erupted fall deposits and Ig1 to later-erupted Ig2 (Table 1; Fig. 5c). The $\Delta^{18}O$(Qz–Mt) temperatures of late erupted crystal-poor low-silica rhyolitic inclusions are comparable with temperatures measured from host crystal-rich rhyolites. The use of lowest- and highest-$\delta^{18}O$ range of quartz from histograms (Fig. 3) for calculating temperature yields 15 °C per 0.2‰; thus, putting 100° ± 20 °C uncertainty on $\Delta^{18}O$(Qz–Mt) temperature determination. There is a remarkably good correspondence of quartz–magnetite and quartz–diopside oxygen isotope temperatures using Chiba et al. (1989) calibrations for Late BT samples containing clinopyroxene (00LV-25, and LV18-18a, Table 1, Fig. 5b), suggesting that oxygen isotope equilibrium is achieved and retained between mean values of quartz, magnetite, and clinopyroxene.

Temperatures based on zircon-melt quench

We also estimated pre-eruptive temperatures of magmas based on zircon saturation (Watson and Harrison 1983)

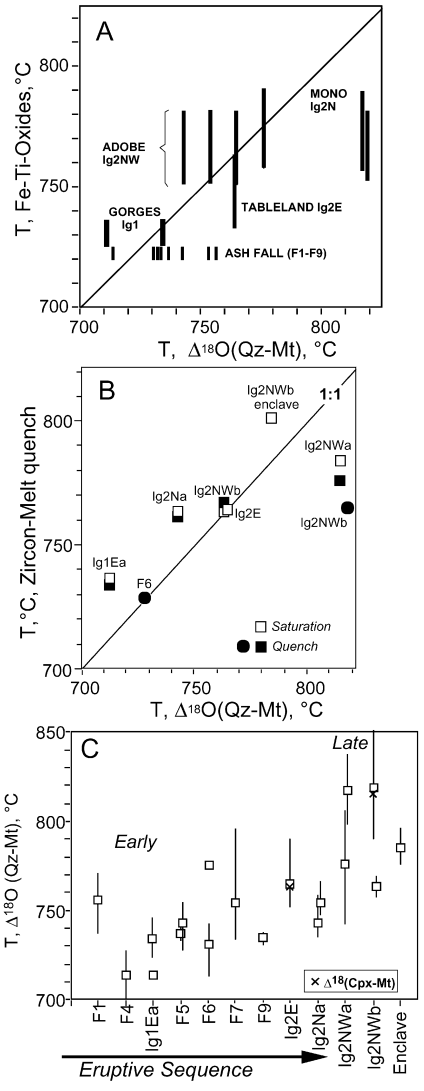

Fig. 5. A Comparison of quartz–magnetite oxygen isotope temperatures, $\Delta^{18}O$(Qz–Mt), this study vs. Fe–Ti oxide cation temperatures from Hildreth (1979) for the same ignimbrite lobes (Fig. 1) and ash fall horizons. **B** Comparison of quartz–magnetite oxygen isotope temperatures vs. pre-eruptive temperature, based on zircon saturation (see Table 2 for analyses, and text for details). *Filled symbols* are temperature of quench based on either measured amount of zircon crystallized (see Table 2, italic data) or ion microprobe analyses of Zr concentration in representative melt inclusions given in Peppard et al. (2001). **C** Calculated oxygen isotope temperatures vs. eruptive sequence (with range of calculated temperature based on $\Delta(Qz–Mt)_{max}$ and $\Delta(Qz–Mt)_{min}$). Notice progressive increase of T in successively erupted units, and good correspondence of $\Delta^{18}O$(Qz–Mt) and $\Delta^{18}O$(Cpx–Mt) temperatures for two samples

by measuring the mass of zircon crystallized, and the rock's crystal content (Table 2; Fig. 5b). Dissolution of four large pumice clasts (200 g) in HF acid yielded 25–66 ppm of zircons (Table 2). These clasts span 90° of Qz–Mt temperature range. Crystal size distributions of these zircons were measured (Appendix 1) and are similar in Early and Late BT, suggesting no net loss or gain of zircons in each sample. Knowing zircon saturation temperatures (Watson and Harrison 1983), Zr concentration in pumice (85–140 ppm, Table 2) minus that in zircon (13–33 ppm), and the correction for rock crystal content, which ranges from 10 to 27 vol%, enables calculation of the quench temperature. One pumice clast from early ignimbrite (Ig1Ea, sample 00LV-27) yielded a low temperature of 734 °C, whereas clasts from three different late ignimbrite lobes yielded progressively higher temperatures: 776 °C (Ig2NWa, LV-748), 767 °C (Ig2NWb, 00LV-3), and 761 °C (Ig2Na, 00LV-751). In three cases (LV-748, 00LV-27, 00LV-751), the calculated zircon-melt quench temperatures are 2–8 °C lower than the saturation temperature calculated from whole-rock analyses; in one case (00LV-3) zircon quench temperature is 5 °C higher. The latter can only be explained by the addition of quartz and feldspar by settling from higher in the magma chamber (e.g., Anderson et al. 2000), to this Late BT sample that diluted whole-rock Zr concentration. The small temperature differences suggest that crystallization of sanidine–plagioclase–quartz in near-eutectic proportions (3–1–3, Hildreth 1979), and crystallization of zircon are congruent in variable-T, and variable P, $f_{(H2O)}$ magma volumes of the BT chamber. This serves as an additional demonstration of the near-eutectic nature of BT and that the temperature variations through the BT magma chamber may vary monovariantly with P and water fugacity. Overall, zircon-melt equilibria are in agreement with Fe–Ti oxides and the $\Delta^{18}O$(Qz–Mt) temperatures (Fig. 5b).

Comparison with quartz–ulvospinel–ilmenite–fayalite (QUILF) thermometry

Lindsley at al. (1991) and Frost and Lindsley (1992) proposed that the appearance of pyroxene in late BT mineral assemblages leads to an QUILF estimate of less than 30 °C, possibly zero, temperature difference between Early and Late BT. Oxygen isotope thermometry and zircon quench temperatures are consistent with an earlier interpretation by Hildreth (1979) of ca. 70 °C, or even higher (Fig. 5b, c) temperature difference between earlier and later erupted BT. We note that Lindsley at al. (1991) and Frost and Lindsley (1992) employed the older eruptive stratigraphy of Hildreth (1979). According to the new eruptive stratigraphy of Wilson and Hildreth (1997), ignimbrite sheet Ig1E (pyroxene-free), and Ig2E (pyroxene-bearing) are coeval or partly coeval in eruptive age with fall deposits F1–F9. There is a consistent 56 °C $\Delta^{18}O$(Qz–Mt), and $\Delta^{18}O$(Cpx–Mt), temperature difference between two pyroxene-bearing samples Ig2E and Ig2NWb (Fig. 5c). In order to reconcile results of the QUILF cation thermometry model of Frost and Lindsley (1992) with isotope thermometry of the present study, we point out that vertical motion of phenocrysts from Early to Late BT magma (e.g., Anderson et al. 2000) has led to faster diffusive equilibration of oxygen, but perhaps incomplete diffusive equilibration of Fe, Ti, and Mg. Below, we explain that $\delta^{18}O$ heterogeneity of some quartz phenocrysts results from sidewall

crystallization and entrapment, and that this process is applicable to pyroxenes if they crystallized near walls.

Isotopic fractionations and $\delta^{18}O$ of Bishop Tuff

Isotope fractionations

In the BT magma chamber, temperature variations are well-constrained based on quartz–magnetite thermometry, and zircon quench temperatures. Therefore, the BT magma chamber provides a natural ''reaction vessel'' to precisely measure the oxygen isotope fractionation between quartz, zircon, pyroxene, and melt at calculated temperatures (Table 3). In the laboratory, it would take more than 10 years of experimentation to produce a 1-μm diffusion profile at 750 °C because of the slow diffusion of oxygen in zircon, even at water saturation (Watson and Cherniak 1997). The sufficiently long residence time inferred from crystal size distribution (see Fig. 9 in Appendix 1) favors the pre-eruptive oxygen isotope equilibration by diffusion and/or solution reprecipitation. The $\delta^{18}O$(Zircon) values in Early ($5.61 \pm 0.14‰$) and Late ($5.82 \pm 0.01‰$) BT show a slight increase with increasing temperature, as required by equilibrium with melt and quartz (Fig. 6). Zircon–quartz fractionation is 1.91–2.45‰ for magmatic temperatures of 700–900 °C in rocks of similar composition from Yellowstone and Timber Mountain, Nevada (Bindeman and Valley 2001, 2002). Rhyolite–pyroxene fractionations (Table 3) are in agreement with experimental quartz–magnetite, quartz–diopside, and quartz–rhyolite fractionations (see below).

The $\delta^{18}O$(melt) value of Bishop Tuff

Because each pumice clast represents a quenched batch of melt originating from a certain P–T loci in the magma chamber prior to eruption, alteration-resistant quartz phenocrysts in these pumice clasts serve as a proxy for the $\delta^{18}O$(melt). The fractionation, Δ(Qz–rhyolite), is less than one per million, and depends on temperature. Δ(Qz–rhyolite) can be calculated from Δ(rhyolite–CO_2 (Palin et al. 1996) and Δ(silica–CO_2) experiments (Stolper and Epstein 1991). Matthews et al. (1994) experimentally demonstrated that silica melt is 0.2–0.4‰ higher in $\delta^{18}O$ than quartz, leading to quartz–rhyolite fractionation of 0.4 (900 °C) to 0.6‰ (700 °C). This is in accord with natural observations on quartz–glass fractionation in similar high silica rhyolites at similar temperatures is 0.5–0.7‰ (Bindeman and Valley 2001). In order to calculate Δ(Qz–rhyolite) for BT, we used the above silica–rhyolite experiments and correction for quartz–silica glass fractionation. The calculated $\delta^{18}O$ value of rhyolitic melt in equilibrium with quartz is 7.8‰ (Fig. 6), and is similar for different pumice clasts from different eruptive units of BT. The measured $\delta^{18}O$(glass) value of densely welded BT at Aeolian Buttes is $7.77 \pm 0.1‰$ (Table 1), which is in near-perfect agreement with the calculated values of $\delta^{18}O$(rhyolite). The resulting $\delta^{18}O$(Qz) 715 °C–$\delta^{18}O$(Qz) 815 °C is 0.11‰, and thus the median difference in $\delta^{18}O$(Qz) values (Figs. 3A and 6) can be entirely explained by temperature. The calculated $\delta^{18}O$(melt) value for low-silica rhyolitic inclusions is $7.95 \pm 0.1‰$, slightly higher, but within error than that of BT rhyolites.

Fractional crystallization of BT magma and variations in crystal content could not lead to variations in $\delta^{18}O$(magma) because BT magma is eutectoid; thus, melt and bulk cumulates have near-similar chemical and isotopic composition. Fractional removal of these bulk

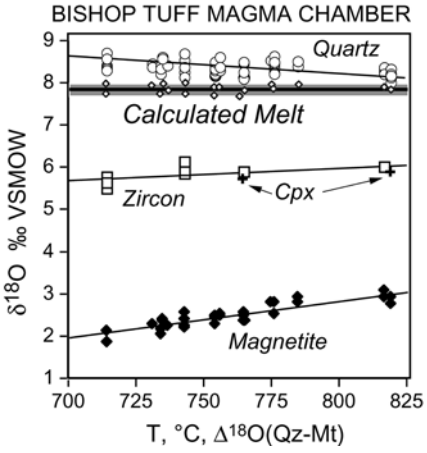

Fig. 6. The $\delta^{18}O$ values of quartz, magnetite, clinopyroxene, and zircon plotted against temperature calculated from $\Delta^{18}O$(Qz–Mt). Notice that the range of $\delta^{18}O$(Qz) can be explained by changing temperature of magma. The calculated values of $\delta^{18}O$(melt) = $7.80 \pm 0.05‰$ are shown (see text for discussion) and do not show any change throughout the Bishop Tuff magma chamber. Notice that variability in $\delta^{18}O$(Qz) and $\delta^{18}O$(Mt) between different portions of BT is caused by different pre-eruptive temperatures whereas the melt is remarkably homogeneous with respect to $\delta^{18}O$

Table 3. Eruptively-quenched rhyolite-mineral oxygen isotope fractionations at calculated temperatures

Sample	T, Δ(Qz–Mt) (°C)	Δ(Qz–Melt) (‰)	Δ(Melt–Zrc) (‰)	Δ(Melt–Cpx) (‰)	Δ(Melt–Opx) (‰)
LV81-18a	819	0.33		2.01	
00LV-748	817	0.44	1.86		
00LV-25	765	0.50		2.07	
00LV-03	763	0.36	1.98		2.18
99LV-751	743	0.45	1.86		
00LV-27	714	0.47	2.21		

cumulates will not lead to change in $\delta^{18}O$. Thus, $\delta^{18}O$(magma) is equal to $\delta^{18}O$(melt).

Therefore, when corrected for temperature, the calculated composition of magma ($\delta^{18}O = 7.8‰$) is identical in Early and Late BT, and in samples ranging from 6 to 11 km deep in vertical position. Likewise, there are no lateral $\delta^{18}O$ variations in the pre-climactic magma chamber, as Plinian fall deposits and ignimbrite sheet Ig1 (erupted from the SE vent) are identical to ignimbrite sheets Ig2NW, erupted mostly from the NW ring fracture (Wilson and Hildreth 1997).

Other large-volume silicic magma systems

Like BT pyroclastic rocks, the earlier (most differentiated) and later-erupted (less differentiated) portions of other large caldera-forming eruptions provide vertical and lateral cross sections through the erupted portions of batholith-scale magma chambers with deep (>1–2 km) eruptive draw-down. For comparison with BT, we analyzed quartz, magnetite, feldspars, and sphene in earlier and later-erupted portions of other large-volume ash-flow sheets from four major calderas (Table 4), of which three are in the western US: Lower Bandelier, Lava Creek, and Fish Canyon Tuffs; plus the Cerro Galan ignimbrite in Argentina. The geology and petrology of these calderas is reported by Self et al. (1986), Lipman (1997), Bachmann et al. (2000, 2002), Hildreth et al. (1984), and Francis et al. (1989). Additionally, we employed duplicated oxygen isotope analyses of the earlier and later portions of Youngest Toba Tuff of Toba Caldera, Indonesia (0.076 Ma, 3,000 km^3) given by Chesner (1988, 1998). Even larger BT volumes of highly differentiated silicic magmas were erupted at these calderas, and they represent different tectonic settings of formation: hot-spot (Yellowstone), rift (Valles), transpressional (Long Valley), or subduction-related (Cerro Galan, Toba, Fish Canyon). Yet, they all share similar features related to processes in large-volume magma chambers: pre-eruptive chemical zoning, and oxygen isotope homogeneity (Table 4).

When $\delta^{18}O$(melt) is calculated from $\delta^{18}O$(quartz) values using $\Delta^{18}O$(Qz–Mt) temperatures and the same procedure as described above for BT, there is no difference in calculated $\delta^{18}O$(melt) between earlier erupted high-silica rhyolitic portions, and later erupted low-silica rhyolitic portions (Fig. 7). Distinct $\delta^{18}O$(melt) for each ash-flow unit suggests derivation from either hydrothermally-altered low-$\delta^{18}O$ rocks (Lava Creek), slightly higher than normal-$\delta^{18}O$ rocks (Bandelier), or supracrustal high-$\delta^{18}O$ rocks (all other units). In the case of Cerro Galan and Fish Canyon Tuffs, eruptive products are more mafic in bulk and unusually crystal-rich (>45 vol% crystals with high-silica-rhyolitic matrix). These so called ''monotonous intermediate'' tuffs do not show zoning with respect to composition and temperature, and may represent remobilized crystal mush in batholith-scale magma chambers (Francis et al. 1989; Lipman et al. 1997; Bachmann et al. 2002). Late erupted Fish Canyon Tuff is only slightly (0.2‰) higher than the earlier-erupted portions. Therefore, we observe remarkable homogeneity of $\delta^{18}O$(melt) values, near analytical precision of oxygen isotope analyses to within ±0.1‰ in other large silicic magma systems. This result confirms that BT is not unusual, but rather is a typical example of oxygen isotope homogeneity.

Discussion

Results of this study demonstrate that BT, other large-volume ash-flow sheets, and granitic batholiths elsewhere could be initially remarkably homogeneous with respect to $\delta^{18}O$. This result is important for interpreting isotopic and chemical evolution during crustal differentiation.

The role of convection

The $\delta^{18}O$ homogeneity of the large BT silicic magma system may indicate that either the BT magma originated from a source homogeneous in $\delta^{18}O$, or that the magma chamber was homogenized by convection. The first possibility is unlikely because the BT could not have been generated 100% as a product of differentiation from homogeneous, ca. 5.8‰ mantle magma. The elevated ''crustal'' oxygen isotope composition of BT requires a significant proportion of crustal partial melting to take place. For example, at least 20–30 wt% of crustal components with $\delta^{18}O = +10‰$ should be present in BT, if it were formed by differentiation of mantle-derived basalt with $\delta^{18}O = +6‰$. Similar proportions can be derived from Nd isotopes (e.g., Halliday et al. 1984; DePaolo et al. 1992). Sedimentary protoliths and partial melts from them are expected to be extremely diverse with respect to $\delta^{18}O$. Country rocks exposed around Long Valley caldera range in $\delta^{18}O$(WR) from 2 to +29‰. The pre-history of melt segregation, and diapiric rise from the lower/middle crust to the pre-eruptive chamber could have contributed to mixing (e.g., MASH model of Hildreth and Moorbath 1988). However, values of $\delta^{18}O$(Qz) in domes of Glass Mountain differ by at least 1‰, and may represent this larger initial $\delta^{18}O$ range of the pre-BT magma chamber. The same degree of variability is seen in rare earth elements (Metz and Mahood 1991), degree of differentiation (Halliday et al. 1984; Christensen and DePaolo 1993), and Nd isotopes (Christensen and Halliday 1996), confirming that during the initial stages of formation of the pre-BT magma chamber, individual pockets of melt had unique trace element and isotopic composition, including a unique Rb/Sr.

Therefore, the second possibility, convective homogenization of the BT magma body, is most likely. This process would require convection for a long enough time to mix any lateral and vertical $\delta^{18}O$ gradients, resulting

Table 4. Oxygen isotope ratios of minerals in upper and lower portions of some large-volume ash-flow tuffs. $\delta^{18}O$(melt) is calculated based on $\delta^{18}O$(Qz) and T (see text). Notice similarity of $\delta^{18}O$(melt) values of Early and Late subunits. In Fish Canyon system pre-caldera units and Early tuff are 0.2‰ lower than Late tuff and postcaldera unit

Tuff sample	Subunit	Caldera/ unit	Volume (m^3)	$^{40}Ar/^{39}Ar$ (Age, Ma)	T range, Δ(QZ–Mt) °C	Crystal content (%)	SiO_2 (wt%)	Qz	$\delta^{18}O$(min) (‰ Mt)	Other[b]	$\delta^{18}O$(melt) (‰)
Lower Bandelier (LBT)		Toledo	600	1.61 ± 0.01[a]							
LBT-10	Late	Ignimbrite			771	25	75	7.81 ± 0.10	2.04 ± 0.05		7.28 ± 0.10
LBT-4	Early	Fall pumice			737	10	77	7.90 ± 0.10	1.74 ± 0.05		7.32 ± 0.10
Fish Canyon (FCT)		La Garita	5000	28.03 ± 0.18							
BFC191	Late				763	35–51	68	8.36 ± 0.01	2.50 ± 0.09	4.34, Sph	7.82 ± 0.15
BFC125	Early				762	35–51	68	8.13 ± 0.06	2.26 ± 0.01	4.19, Sph	7.60 ± 0.15
BFC83	Pre-caldera	Pagosa Peak	> 200	29.93 ± 0.18	751	45	68	8.18 ± 0.10	2.18 ± 0.10	4.67, Sph	7.63 ± 0.10
BFC115	Post-caldera	Nutras Creek	< 1	28.06 ± 0.16	701	44	68	8.41 ± 0.10	1.78 ± 0.10		7.83 ± 0.10
Lava Creek (LCT)		Yellowstone	1000	0.640 ± 0.002							
LCT-2	Late	Member B			912	15–25	73	6.40 ± 0.05	1.89 ± 0.13	5.49, San	5.98 ± 0.05
LCT-3a	Early	Member A			800–850	5–20	77	6.46 ± 0.10		5.34, San	5.98 ± 0.10
Cerro Galan (CG)		Cerro Galan	1000	2.03 ± 0.07		42–49	68				
GG-1	Late				724			9.96 ± 0.02	3.64 ± 0.04	8.50, Pl	9.36 ± 0.02
GG-2	Early				726			10.02 ± 0.04	3.72 ± 0.06	8.42, Pl	9.42 ± 0.04
Yongest Toba (YTT)[a]		Toba	2800	0,074							
	Late				761	30–40	69	9.60 ± 0.10	4.00 ± 0.05	8.25, Pl	9.06 ± 0.10
	Early				787	12–25	77	9.58 ± 0.13	3.70 ± 0.05	8.15, Pl	9.05 ± 0.13

[a]Lower Bandelier age is from Spell et al. (1996); Lava Creek age is from Lanphere et al. (2001, written communication). Fish Canyon ages are from Bachmann et al. (2000); Cerro-Galan Rb/Sr age is from Francis et al. (1989). Oxygen isotope analyses and sample descriptions for Toba are from Chesner (1988, 1998)
[b]*Sph* sphene, *San* sanidine, *Pl* plagioclase

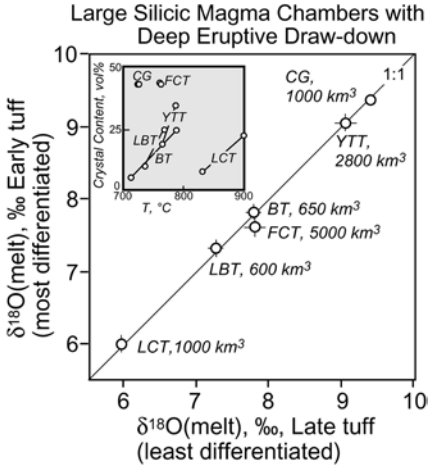

Fig. 7. Comparison of oxygen isotope values of shallow (most differentiated and early erupted) vs. deep (least differentiated and later erupted) portions of major Quaternary ignimbrite sheets of the world demonstrates vertical homogeneity in δ^{18}O(melt) values for erupted portion of each ash-flow unit. The *inset* shows average crystal content vs. temperature. See Table 4 for analyses and text for discussion

from the segregation, emplacement, and the initial assimilation of varying country rock lithologies.

Mechanisms of convection: sidewall crystallization

In the BT magma chamber, as in many other chambers, the convective regimes and patterns were likely changing through time, as convection even in rhyolitic systems is a rapid process with convective velocities of millimeters to centimeters per hour (e.g., Trial and Spera 1990). For the purpose of this paper, the basis for selecting a specific convective model is twofold: (1) the model should explain large-scale oxygen isotope homogeneity of BT batholith-scale magma chamber achieved during its lifetime; and (2) it should explain isotopic heterogeneity of some phenocrysts that could persist for only 10^2-10^4 years (see Appendix 1 and discussion below). A general sidewall crystallization model (Fig. 8) would satisfy both requirements. For eutectoid high-silica systems such as Bishop Tuff, with high viscosity, and low diffusivities, thermal and compositional changes in density related to crystallization are expected to be negligible. Instead, we suggest that near-wall crystallization results in variable gas bubble exsolution that leads to a decrease in bulk density and the upward motion of a gas-richer boundary layer.

The large range in δ^{18}O values of individual quartz crystals may represent sidewall crystallization or entrapment (Fig. 8). Quartz crystals from the mushy crystal rind around BT magma chamber may be more variable in δ^{18}O because of (1) the possibility of xenocrystic contamination as a result of partial melting of variable δ^{18}O wall rocks, and (2) the rapid exchange of oxygen with country rocks of differing lithology and δ^{18}O.

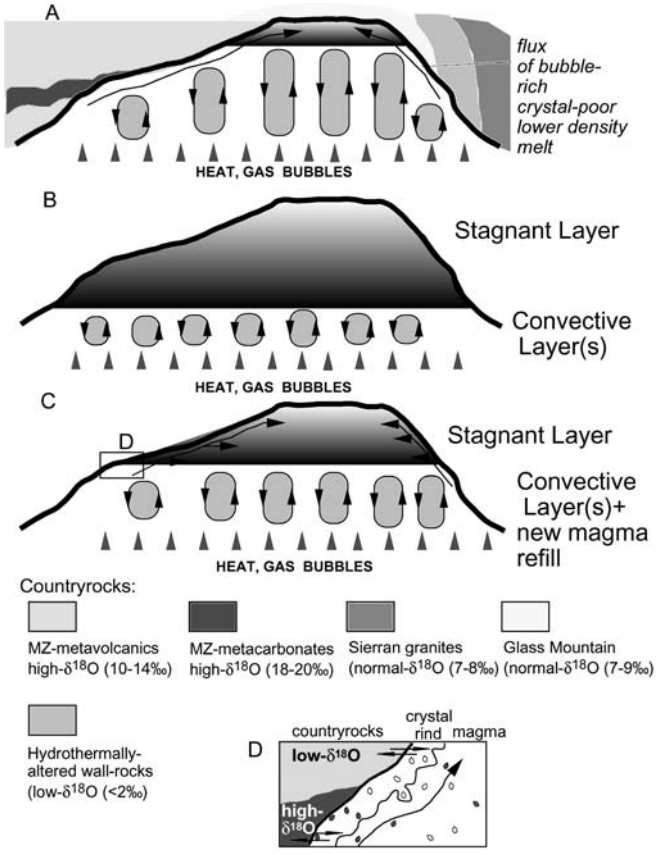

Fig. 8A–D. Proposed model of convective cooling and gas release, and formation of a stably-stratified eutectoid magma chamber parental of Bishop Tuff. **A** Whole-chamber convection homogenizes magma with respect to oxygen isotope ratios. **B** Crystallization, differentiation, and effervescence lead to accumulation of more differentiated, and bubble-rich lighter eutectoid magma near chamber's roof; dominantly conductive cooling of a layer heated from below by inputs of more mafic magma, and by latent heat of crystallization of crystal mush. The upper portion undergoes crystal fractionation. **C** Pre-0.76 Ma configuration tens of thousands of years prior to caldera collapse. Refill by more mafic, volatile, and Sr-, Ba, and Zr-rich magma causes thawing and disturbance of crystal mush, magma mixing, and crystal settling into the hybrid melt. **D** A fragment of a sidewall showing oxygen isotope exchange through the crystal mush

Expectedly, sidewall crystallization and residence would also affect trace element, and other isotopic systems. The $^{87}Sr/^{86}Sr_i$ in individual pumice clasts (Knesel and Davidson 1997), feldspars (Duffield and Ruiz 1998), and in quartz-hosted melt inclusions (Christensen and Halliday 1996) from the same stratigraphic unit exhibit significant ranges from 0.706 to 0.712. Crystallization and residence of quartz phenocrysts near chamber walls may enhance the proportion of inherited Ar (e.g., Winick et al. 2001), derived from older country rocks. Trace element and volatile concentrations of quartz-hosted melt inclusions reported by Lu (1991), Dunbar and Hervig (1992), Wallace et al. (1999), and Anderson et al. (2000) exhibit scatter around delineated trends, suggesting variable amounts of crystallization and fluid exsolution, even in neighboring melt inclusions within a

single phenocryst. In similar rhyolitic systems elsewhere, feldspars preserve a memory of assimilation of high-$^{87}Sr/^{86}Sr$ wall rocks (Wolff et al. 1999). All these observations can be best explained if there were local gradients in the degree of crystallization and gas exsolution near magma chamber walls. Thus, in competition with the homogenizing process – convection – there is a relatively rapid process – sidewall crystallization – which locally generates the heterogeneity on a thousands-of-years or shorter time scale.

The argument against sidewall residence of quartz and other phenocrysts often includes the lack of crystal aggregates (e.g., Anderson et al. 2000). However, material properties remain uncertain: viscosity, yield strength, of three-phase mixture gas + rhyolitic melt + crystals, and their dependence on temperature and water content. The results of the present study, along with a growing body of other evidence for sidewall crystallization and crystal storage, suggest that exsolved gas bubbles near chamber walls play an important role in keeping crystals apart, as well as controlling viscosity and rheology of the three-phase crystals + gas + melt mixture, which is ultimately responsible for crystal entrapment, storage, and release. Wallace et al. (1999) estimated that gas bubbles may constitute up to 5 vol% in the interior parts of BT magma chamber, and we suggest that gas proportion may be progressively higher toward chamber's walls.

Longevity of the BT magma body and timescales

The overall homogeneity of the BT magma chamber also allows estimates of its longevity, based on the time required for diffusive equilibration. One experimental study on ^{18}O diffusion exists to our knowledge with hydrous high-silica rhyolite similar to BT (Stanton et al. 1989), but see also Wendlandt (1991), Zhang et al. (1991; Liang et al. (1996), and Tinker and Lesher (2001) for relevant discussions of oxygen diffusion in silicate melts. There could be a strong influence of dissolved water species on oxygen self-diffusion in highly-polymerized silicic melts, and ^{18}O diffusion coefficients could be only 50 times smaller than diffusion coefficients for water in hydrous silicate melts ($\sim 10^{-7}$ cm^2/s, e.g., Stanton et al. 1989; Zhang et al. 1991). As a result, variations in $^{18}O/^{16}O$ ratios in melt would anneal 1–2 orders of magnitude faster than concentrations of silicon and other major elements (e.g., 10^{-9} cm^2/s for rhyolites with 6 wt% of water, e.g., Baker 1991). However, convection is required to homogenize $^{18}O/^{16}O$ in >650 km^3 BT magma body. When convection mixes different parts of rhyolite to a characteristic 1-m scale, homogenization of $^{18}O/^{16}O$ by "wet" oxygen diffusion can happen in $<40{,}000$ years. Therefore, the efficacy of mixing on a 1-m-scale can be achieved relatively fast, but it is dependent on the goodness of mixing: the scale of convective dispersal.

The model of Oldenburg et al. (1989) for silica homogenization can be used to estimate the characteristic timescales at size, viscosities, heat fluxes, and diffusivities of the BT magma chamber. Dispersion to the $\sim$1-m scale can be achieved over a long time scale of 10^5 to 10^6 years. We conclude that, because $^{18}O/^{16}O$ in the BT magma body is homogeneous on a cubic kilometer-scale, convection has been effective in dispersing the magma to meter-scale, and that the oxygen isotope homogeneity of 650 km^3 of BT and other large magma bodies (Fig. 7) supports a long residence time of at least several hundred thousand years. If time is shorter ($<10^5$ years), natural evidence elsewhere suggests that oxygen isotope homogeneity is not achieved in similar $>1{,}000$-km^3 tuff units (Bindeman and Valley 2002).

Pre-eruptive compositional gradients and crystal zoning

Any convective model should explain BT zoning in many other parameters: 100°/4 km temperature gradient, factor of two variations in Zr content and other trace elements, increase of crystal content from 5 to 25%, variations in $^{87}Sr/^{86}Sr_i$, and volatile contents.

Given the inferred long life span ($>10^5$–10^6 Ma) of the pre-climactic BT magma body, and similar sized magma bodies (Table 4), we fundamentally favor a time-integrated multi-component model that includes both long-term, and short-term timescales. Our proposed model of sidewall crystallization and receding convection is capable of generating gradients of some elements, homogenize $^{18}O/^{16}O$ in the interior of the magma body, and can also create compositional zoning. The upper part of the magma chamber becomes progressively stagnant and stabilized by upward-increasing gas bubble concentration, and downward-increasing crystal content. Other gradients (e.g., Rb/Sr) developed later as a result of feldspar fractionation from the upper portion of a stagnant magma. Roofward increase in $^{87}Sr/^{86}Sr_i$ could be explained by both assimilation of high-$^{87}Sr/^{86}Sr$ country rocks (Duffield et al. 1995, Knesel and Davidson 1997), and the effects of in-situ aging caused by extremely high $^{87}Rb/^{86}Sr$ in a chamber with complex geometry (e.g., Halliday et al. 1989).

However, crystal zoning, and crystal-size distributions (Appendix 1) suggest shorter timescales. The long lifeline of the BT magma chamber does not permit preservation of $\delta^{18}O$ variations in quartz phenocrysts. At water saturation, $^{18}O/^{16}O$ differences in 3-mm-diameter quartz phenocrysts should anneal in several thousand years at 750 °C (Farver and Yund 1991); it would take an order of magnitude longer in dry conditions (see Cole and Chakraborty 2001). In any case, the preservation of $\delta^{18}O$ heterogeneity in some quartz phenocrysts suggests that they have been entrapped, recrystallized, and diffusively exchanged shortly (10^2–10^4 years) before the caldera-forming eruption. Additionally, late BT is characterized by a rimward increase in Sr, Ba, and Ti concentration in feldspar phenocrysts (Lu 1991; Dunbar and Hervig 1992; Anderson

et al. 2000), and distinct bright-CL rims on quartz phenocrysts (Peppard et al. 2001). These characteristics are all consistent with Early phenocrysts sinking into the progressively more Zr-, Sr-, Ba-rich hybrid melt that would take $\sim 10^4$ years at typical BT viscosities (Appendix 1). Moreover, the preservation of such zoned crystals in ~800 °C Late BT magma suggests similar $\sim 10^4$ years timescales, as do their CSD (Appendix 1), far shorter than the lifeline of the BT magma body.

In order to reconcile long and short timescales, we suggest that compositional and thermal gradients in the erupted upper portion of the pre-0.76 Ma BT magma body are relatively short lived and reflect pre-eruptive configuration, and possibly a most recent episode of chamber refill by a new batch of initially hotter, high-Zr-, Sr-, and Ba-rich magma. This refill 10^3–10^4 years before 0.76 Ma caldera-forming eruption of BT could have caused extrusion of the youngest Glass Mountain lavas that are identical to BT in $\delta^{18}O$ (Fig. 2, see above), and erupted shortly (10^4 years) before BT (Fig. 2). The new magma mixed with the lower portions of BT magma body and thawed near-wall mushy zones causing downward crystal settling into progressively hotter, Zr-, Sr-, and Ba-richer hybrid melt (Fig. 8C, D). The following history of the BT magma chamber is the history of progressive thermal and diffusive exchange that was aborted at 0.76 Ma by the caldera-forming eruption.

The present study demonstrates that large silicic magma chambers and granitic batholiths are homogenized by convection, followed by periods of stagnation of their apical portions, which are often disturbed by periodic refill from below. Gradients in other parameters are time integrated and are both long-lived, and short-lived, and, expectedly, reflect mixing because of refill and crystal fractionation. One can hypothesize if formation of these gradients in the upper stagnant portion of pre-climactic magma chambers, and climactic caldera-forming eruptions are genetically-related. A thick stagnant portion in the upper portion of the magma chamber is capable of producing significant gas over-pressure because it serves as a kinetic barrier (due to of higher viscosity) and possibly a rheological trap (because of the melt structure and/or higher crystallinity near the roof) for gas bubble exsolution and flotation from below. The higher proportion of gas bubbles in the upper portion of the BT magma chamber lowers the bulk magma density (e.g., Wallace et al. 1999). Bubble flotation leads to an additional >100 bar overpressure in magma chambers, which is proportional to the depth of their rise (e.g., Steinberg et al. 1989; Bindeman and Podladchikov 1993), whereas gas loss into the overlying country rocks decreases the chamber overpressure. Collectively, pre-conditions are set for roof collapse and caldera-forming eruption, which could have been triggered by tectonic forces along the major Sierran fault.

Acknowledgements We are grateful to Fred Anderson for providing an important suite of samples (BT-, LV-, BC-) previously analyzed for trace elements and volatile content, Roy Bailey for 1998 field overview of Long Valley caldera, Mike Spicuzza for advice during isotope analyses, Jade Star Lackey for help with sample collection, and Colin Wilson for suggesting sample localities. Olivier Bachmann kindly provided samples of Fish Canyon Tuff, Carsten Schirnick and Paul van den Bodaard provided samples of Cerro Galan ignimbrite, Philip Kyle suggested the locality to sample Lower Bandelier Tuff, Craig Chesner provided data from his dissertation for Fig. 7. Reviews by Paul Wallace, Shan de Silva, and Arnd Heumann, and editorial suggestions by Tim Grove, are gratefully acknowledged. This research was supported by DOE (FG02-93ER14389).

Appendix 1

Zircon and quartz crystal size distribution in Bishop Tuff

This section deals with the crystal size distribution (CSD) of quartz and zircons in seven stratigraphically different samples of BT. We attempt to examine the general shape of CSD profiles, find a correlation of CSD with the relative progress of zircon and quartz crystallization, estimate crystallization time and CSD longevity at assumed growth rates, and find evidence for fractionation in the magma chamber (Fig. 9). We also address the question of concave-down CSD and the role of CSD annealing as a function of decreasing nucleation rates and Ostwald ripening.

Two hundred grams of uncrushed pumice was dissolved in cold 48% HF for 5–10 min and yielded optically unetched to very weakly-etched crystals of quartz, and variably etched feldspar. Additional and prolonged (several days) HF dissolution yielded only zircons in the residue. CSD measurements were performed using the NIH Image program and included the measurements of length and the width of each crystals. Only doubly-terminated whole quartz crystals were measured; these

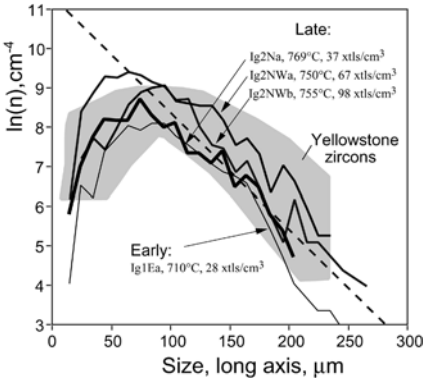

Fig. 9. Zircon crystal size distribution, expressed as the logarithm of population density ln(n) vs. crystal length in four individual pumice clasts; *n* is the number of crystals of length *L* (sample bin = 10 μm), in a 1-cm^3 unit volume of magma. Normalization to unit volume and a bin size gives dimension of cm^{-4}. Each curve is based on measurements of 350 to 501 crystals. See Table 2 for analyses, and $\Delta^{18}O$(Qz–Mt) temperatures. *Dashed line* indicates calculated isochron for a zircon population crystallized at a constant rate of using the relation: slope $= -1/$(growth rate × residence time) (Cashman and Marsh 1988)

crystals constituted from 70% of quartz phenocrysts in Early erupted BT to only 40–50% in Late erupted BT. We attribute the greater fragility of later-erupted quartz phenocrysts to the greater depths and temperatures of their pre-eruptive location deeper in the magma chamber, which results in syneruptive decrepitation of quartz-hosted, volatile-bearing melt inclusions. Although pre-selection of only doubly-terminated quartz may introduce some bias in the quartz CSD, visual examination shows that phenocrysts of different sizes are cracked in a similar fashion; only the least abundant, smallest crystals appear less affected.

The measured CSD for quartz and zircons show a similar log-normal concave-down pattern when plotted on a standard diagram of the natural logarithm of population density vs. crystal length. The population density is calculated per unit volume, per length bin size, and thus measured in units of cm^{-4} (Fig. 10). Concave-down profiles are not commonly observed in volcanic systems (e.g., Cashman and Marsh 1988), but are more common in plutons (Eberl et al. 1998), and migmatites (Nemchin et al. 2001) that show prolonged cooling and a progressive decrease in nucleation rates. Although it was very difficult to perform quantitative CSD measurements on sanidine and plagioclase phenocrysts, optical examination of crushed pumice clasts suggests a similar deficiency of smaller crystals less than 0.8 mm, and a lack of crystals less than 0.3 mm.

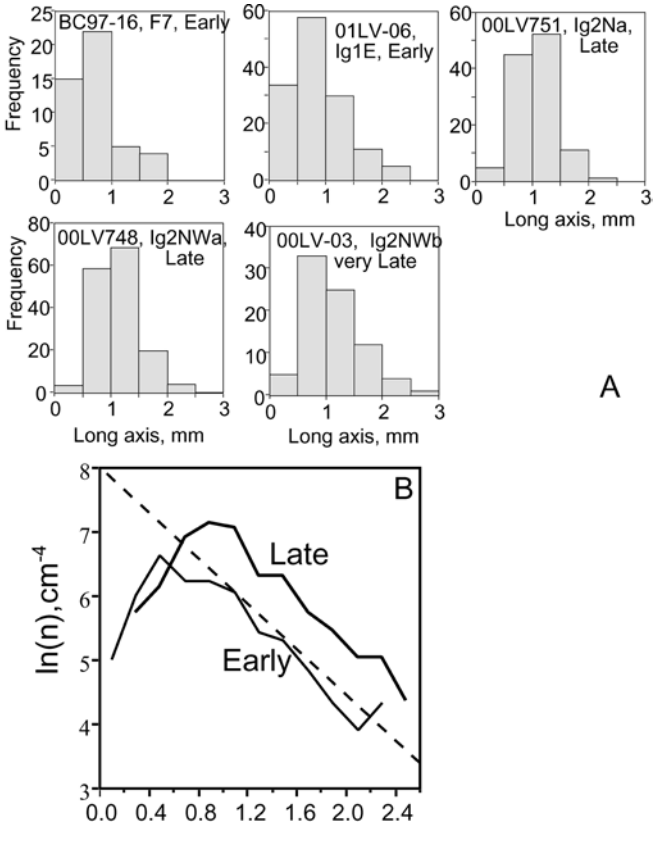

Fig. 10A–B. Quartz crystal size distribution in Bishop Tuff. **A** Histograms of quartz sizes in five samples of Bishop Tuff. **B** Quartz crystal size distribution for Early and Late Bishop Tuff. Notice systematically larger sizes of quartz in Late BT and deficiency of small crystals in all samples. *Dashed line* indicates calculated isochron of 57,000 years for a quartz population with a constant growth rate 10^{-11} cm/s

No distinctive difference in CSD patterns of zircons between different ignimbrite lobes was detected as a function of temperature, amount of zircon present, or zirconium concentration. However, CSD for zircons in Early ignimbrite Ig1E plots at the lower end of Late ignimbrites, consistent with lower Zr abundance, and vol% of zircons (Table 2) in the former. The number of zircons per 1 cm^3 of vesicle-free BT ranges from 28 in Ig1E, to 98 in Ig2NWb. There is no evidence for the accumulation of larger zircons in the later erupted, more Zr-rich portions of BT, although the number of zircons per cubic centimeter increases threefold. This trend is parallel to the increase in total Zr in the sample [zircon contains only 20–30% of total Zr in a rock and most zirconium (80%) resides in glass, Table 2]. Therefore, the zircon CSD patterns are consistent with in-situ growth of zircon in each parcel of the BT magma.

The CSD pattern of zircons in BT are similar to those observed in Yellowstone rhyolites (Bindeman and Valley 2001; Bindeman et al. 2001), when plotted on the same, volume- and length-normalized diagram. It seems that concave-down profiles are typical for zircon CSDs. We attribute zircon concave-down CSD pattern to indicate the decreasing rate of nucleation in combination with Ostwald ripening (dissolution of smaller crystals and growth of larger crystals) at near-equilibrium in eutectoid BT and other similar magmas.

Quartz CSDs (Fig. A2b) are similar (concave-down), and demonstrate a lack of crystals smaller than 0.1 mm in diameter, and a deficiency of crystals in the 1–0.1 mm range in comparison to the dashed-line that would be consistent with their crystallization as a single population with exponentially increasing nucleation rates. There is a systematic difference in quartz CSD between Early and Late BT (Fig. A2b). Quartz CSD in later-erupted, crystal-richer BT has larger mean crystal size and fewer small (< 0.5 mm) crystals. Such observations are consistent with the model of Anderson et al. (2000) for crystal settling, which causes the accumulation of larger crystals at the bottom of the erupted portion of BT, 3–4 km down. It would take 10,000 years for a 3-mm-diameter quartz to sink 3 km through 5×10^5 poise rhyolitic melt at Stokes velocity. Yet, the lack of small quartz crystals characterizes earlier erupted portions of the BT as well, and it is too dramatic to be explained by crystal removal/addition. Swanson and Fenn (1986) demonstrated in experiments that the lack of small crystals is a result of suppressed nucleation in silicic magmas, as quartz tends to form spherulites with feldspar, or overgrowth on larger quartz crystals. Smaller crystals of quartz and zircon would also dissolve preferentially if they crystallized in mash near chamber walls (Fig. 8d), and if there was a thawing episode by hotter magma prior to caldera collapse. Collectively,

nucleation kinetics, Ostwald ripening in mash, and dissolution of smaller crystals by periodic thawing have lead to concave-down CSDs that are viewed as time-integrated patterns.

Zircon and quartz CSDs can be used to estimate average residence times, although they are a strong function of the assumed growth rates. Zircon CSDs (Fig. A1) suggest 10,000–100,000 years residence for zircon crystallization at nominal growth rates of 10^{-14} to 10^{-15} cm/s (Watson 1996), which would be consistent with analytically indistinguishable U–Pb ages of cores and rims of BT zircons ($\pm$10,000–45,000 years, Reid and Coath 2000). For quartz, the slopes of CSDs yield 16 to 160 years residence at "fast" nominal growth rates of 10^{-10} to 10^{-11} cm/s (e.g., Swanson and Fenn 1986), or 40,000 years at "slow" 4×10^{-14} cm/s nominal growth rate (e.g., Christensen and DePaolo 1993). Collectively, both quartz and zircon residence times are short compared with BT lifeline. However, they are commensurate with diffusive timescales that are necessary to equilibrate oxygen in quartz, and Sr and Rb in sanidine (see profiles in Dunbar and Hervig 1992; and Anderson et al. 2000 at "wet" diffusion coefficients of Farver and Yund 1991 and Giletti 1991). Although strongly model-dependent, all these estimates point to short timescales (10^2–10^4 years) as compared with the inferred lifeline of the BT magma chamber (3×10^5 to 2×10^6 years), or geologically certain 2×10^6-year lifetime of the Glass Mountain-BT magma system. We conclude that these short times reflect the near wall crystallization and convection phenomena described above (Fig. 8).

Appendix 2 (Information for the supplementary electronic data)

Bishop Tuff–Glass Mountain magma system

The $^{40}Ar/^{39}Ar$ and K/Ar dating of volcanic rocks in and around Long Valley Caldera (Bailey et al. 1976; Mankinen et al. 1986; Mahood et al. 2000; Sarna-Wojcicki et al. 2000) creates a framework for petrological modeling and interpretation. Below, a brief petrologic description of the 2.1-Ma eruptive sequence is given.

Glass Mountain

Basaltic volcanism around the present-day Long Valley Caldera started 3.4 million years ago (Bailey 1989). The oldest manifestations of rhyolitic magmatism at 2.1 Ma are displayed in the early extrusive domes of Glass Mountain (GM, >50 km^3). Petrologically, the rhyolites of GM comprise a sequence of most chemically evolved older domes (2.1–1.2 Ma), and less evolved younger domes (1.2–0.79 Ma, Fig. 1, bottom), which become compositionally more homogeneous and voluminous with youth. The youngest rhyolites are similar to high-silica rhyolites of the Bishop Tuff with respect to major and trace elements, and Sr and Nd isotopes (Halliday et al. 1989; Metz and Mahood 1991; Davies and Halliday, 1998). GM lavas and BT overlap in their Pb isotopic composition (Halliday et al. 1989; Heumann 1999). Young GM lavas and BT have similar ϵ_{Nd} of around –1, although Older GM lavas are characterized by more variable and lower ϵ_{Nd} of around –3 (Halliday et al. 1984, 1989; Davies and Halliday 1998). $^{87}Sr/^{86}Sr_i$ is high in GM and shows significant variations in old GM lavas (0.707–0.719), mostly because of highly variable Rb/Sr ratios, but younger GM lavas have $^{87}Sr/^{86}Sr_i$ largely similar to BT (0.706–0.709). Some feldspar (Davies and Halliday 1998) and quartz phenocrysts (Christensen and Halliday 1996) in early BT are interpreted to have been derived from both old and young GM lavas, based on their distinctive ϵ_{Nd} and $^{87}Sr/^{86}Sr_i$. The $^{87}Sr/^{86}Sr$ (Christensen and Halliday 1996) and $^{40}Ar/^{39}Ar$ age in quartz-hosted melt inclusions (Bogaard and Schirnick 1995), along with regional Rb–Sr isochrons in GM (Halliday et al. 1989; Davies and Halliday 1998), suggest prolonged magma residence times ($>3\times10^5$–10^6 years) in GM–BT magma system. Such long residence times require a constant flux of basaltic magma of $\sim$0.01 km^3 per year (Christensen and DePaolo 1993) to keep the system molten. Regardless of the interpretation of geochronologic information, isotopic ratios and trace elements suggest Young GM as a precursor magma chamber for BT.

Bishop Tuff

Eruption of BT at 0.76 Ma produced at least 650 km^3 of ignimbrite and ash, which covered most of the western US (Sarna-Wojcicki et al. 2000), and created a 30×16 km caldera. Based on the eruptive volume and caldera size, the vertical subsidence following the caldera collapse was estimated to be as much as 2 km (Hildreth and Mahood 1986). Melt inclusions and gas-saturation studies however, suggest an even deeper eruptive drawdown (from 6 to 11 km; Wallace et al. 1999; Anderson et al. 2000), which can be explained by a funnel-like geometry of the magma chamber (Wallace et al. 1999).

BT is comprised of high- to low-silica rhyolites. Mafic magmas were not erupted with BT. Trachytic pumice clasts were recently discovered by Wes Hildreth among the latest erupted crystal-rich rhyolites at Aeolian Buttes (Fig. 1). These nearly aphyric 5–10 cm clasts constitute less than 1 vol% of pumice clasts in this locality, and exhibit textural evidence of co-eruption and mingling with rhyolite. They contain higher whole-rock Ba, Sr, Zr, Ti, and LOI (sample 01LV-4, Table 2), in excellent agreement with the end member composition inferred from melt inclusion studies by Hervig and Dunbar (1992).

Wilson and Hildreth (1997) offered a new stratigraphy of BT, which is based on the lateral correlation of fall deposits, lithic fragments, and mineral assemblages. This new stratigraphy suggests a more complicated

eruption dynamics, which includes nearly coeval eruption of airfall deposits and ignimbrite Ig1, and describes new dynamics of ring fracture propagation. This new stratigraphy is useful for eruption chronology, and also for gaining insights into the position of each particular pumice clast (e.g., lateral vs. vertical) in the magma chamber shortly prior to eruption, and we have employed the new stratigraphy in this work.

Post-caldera lavas and domes

Following caldera collapse at 0.76 Ma, rhyolitic magmatism continued within Long Valley caldera (Bailey 1989; Heumann and Davies 1997; Heumann 1999). Early post-caldera aphyric rhyolites (750–650 ka, > 75 km^3) were erupted and uplifted by resurgence in the center of the caldera, and also intruded as sills in intracaldera BT (McConnell et al. 1995; Table 1). After a 100,000 year quiescence, two groups of moat rhyolites, low-silica, and high-silica, erupted around the resurgent dome (Mankinen et al. 1986). The youngest moat rhyolites erupted 100,000 years ago together with basaltic and quartz-latitic lavas in the western part of caldera. This volcanism was followed by the genetically-unrelated silicic Mono-Inyo Domes (40–41 ka, Bailey 1989). The trace elements, progressively lower $^{87}Sr/^{86}Sr_i$–$^{206}Pb/^{204}Pb$, and higher ϵ_{Nd} suggest that post-caldera volcanism was driven by the addition of a new mantle-derived component that underwent fractionation to dacites and suffered a lesser degree of crustal contamination (Heumann and Davies 1997; Heumann 1999). Little basalt has erupted within the caldera; rare vesiculated basaltic enclaves are found in 650-ka obsidianic rhyolites in eastern Resurgent Dome. These hybridized enclaves serve as evidence that basalt underplating was a heat source beneath the layer of the BT magma body. Post-caldera mafic magmas erupted in the western moat (Mahood et al. 2000), on the caldera rim (Mammoth Mountain, 0.2 Ma), and extra-caldera (Devils Postpile, 0.3 to 0.2 Ma), and more recently at Mono Lake (13.3 ka, Bailey et al. 1976).

Country rocks

Long Valley caldera is surrounded by Paleozoic and Mesozoic metavolcanic and metasedimentary rocks, as well as Mesozoic Sierra Nevada granitoids (Bailey 1989). Many of these country rocks are present as clastic inclusions throughout the BT and were used to infer the sequence of caldera-ring fracture propagation (Hildreth and Mahood 1986; Wilson and Hildreth 1997). Sierra Nevada granitoids in the vicinity of Long Valley have regionally defined δ^{18}O(WR) values for the "Western Volcanic Zone" of $+8$ to $+9‰$ (Masi et al. 1981; Lackey et al. personal communication 2002). Oxygen isotope studies of metasedimentary rocks showed expected large variability, from $+8$ to $+29‰$ in some metacarbonates of the Mt. Morrison roof pendant (Smith and Suemnicht 1991; Lackey and Valley 1999) to $2‰$ in hydrothermally altered volcanic rocks below BT exposed at depths of up to 2 km in drill holes (McConnell et al. 1997). Plutonic and metasedimentary rocks also show a wide range in Sr isotope compositions (0.706–0.725), usually exceeding that of BT (Goff et al. 1991).

References

Anderson AT, Davis AM, Lu F (2000) Evolution of Bishop Tuff rhyolitic magma based on melt and magnetite inclusions and zoned phenocrysts. J Petrol 41:440–473

Bachmann O, Dungan MA, Lipman PW (2000) Voluminous lava-like precursor to a major ash-flow tuff: low-column pyroclastic eruption of the Pagosa Peak Dacite, San Juan volcanic field, Colorado. J Volcanol Geotherm Res 98:153–171

Bachmann O, Dungan MA, Lipman PW (2002) The Fish Canyon magma body, San Juan volcanic field, Colorado: rejuvenation and eruption of an upper crustal batholith. J Petrol 43(8) (in press)

Bailey RA (1989) Geologic map of the Long Valley Caldera, Mono-Inyo craters volcanic chain, and vicinity, eastern California. US Geological Survey Misc Inv Series, Map I-1933, 1:62,500

Bailey RA, Dalrymple GB, Lanphere MA (1976) Volcanism, structure, and geochronology of Long Valley caldera, Mono County, California. J Geophys Res 81:725–744

Baker DR (1991) Interdiffusion of hydrous dacitic and rhyolitic melts and the efficacy of rhyolite contamination of dacitic enclaves. Contrib Mineral Petrol 106:462–473

Bergantz GW (1995) Changing techniques and paradigms for the evaluation of magmatic processes. J Geophys Res 100(B9):17603–17613

Bindeman IN, Podladchikov YY (1993) Inclusions in volcanic rocks and a mechanism for triggering volcanic eruptions. Modern Geol 19:1–11

Bindeman IN, Valley JW (2001) Low-δ^{18}O rhyolites from Yellowstone: magmatic evolution based on analyses of zircons and individual phenocrysts. J Petrol 42:1491–1517

Bindeman IN, Valley JW (2002) Rapid generation of large volume low-δ^{18}O, and high-δ^{18}O magmas at Timber Mountain/Oasis Valley caldera complex, Nevada. Geol Soc Am Bull (in press)

Bindeman IN, Valley JW, Wooden JL, Persing HM (2001) Post-caldera volcanism: in situ measurement of U–Pb age and oxygen isotope ratio in Pleistocene zircons from Yellowstone caldera. Earth Planet Sci Lett 189:197–206

Bogaard PVD, Schirnick C (1995) $^{40}Ar/^{39}Ar$ laser probe ages of Bishop Tuff quartz phenocrysts substantiate long-lived silicic magma chamber at Long Valley, United States. Geology 23:759–762

Cashman KV, Marsh BD (1988) Crystal size distribution (CSD) in rocks and the kinetics and dynamics of crystallization II: Makaopuhi lava lake. Contrib Mineral Petrol 99:292–305

Chesner CA (1988) The Toba tuffs and caldera complex, Sumatra, Indonesia: insights into magma bodies and eruptions. PhD Thesis, Michigan Technological University, Houghton

Chesner CA (1998) Petrogenesis of the Toba Tuffs, Sumatra, Indonesia. J Petrol 39:397–438

Chiba H, Chacko T, Clayton RN, Goldsmith JR (1989) Oxygen isotope fractionations involving diopside, forsterite, magnetite, and calcite –application to geothermometry. Geochim Cosmochim Acta 53:2985–2995

Christensen JN, DePaolo DJ (1993) Time scales of large volume silicic magma system: Sr isotopic systematics of phenocrysts and glass from the Bishop Tuff, Long Valley, California. Contrib Mineral Petrol 113:100–114

Christensen JN, Halliday AN (1996) Rb–Sr ages and Nd isotopic compositions of melt inclusions from the Bishop Tuff and the

generation of silicic magma. Earth Planet Sci Lett 144:547–561
Cole DR, Chakraborty S (2001) Rates and mechanisms of isotopic exchange. In: Valley JW, Cole DR (eds) Stable isotope geochemistry. Min Soc Am, Rev Mineral Geochem, 43:83–225
Davies GR, Halliday AN (1998) Development of the Long Valley rhyolitic magma system: Sr and Nd isotope evidence from glasses and individual phenocrysts. Geochim Cosmochim Acta 62:3561–3574
Davis JC (1973) Statistics and data analysis in geology. Wiley, New York
DePaolo DJ, Perry FV, Balridge WS (1992) Crustal versus mantle sources of granitic magmas: a two-parameter model based on Nd isotope studies. Trans R Soc Edinb 83:439–446
de Silva SL, Wolff JA (1995) Zoned magma chambers: the influence of magma chamber geometry on sidewall convective fractionation. J Volcanol Geotherm Res 65:111–118
Dobran F (2001) Volcanic processes: mechanisms in material transport. Kluwer, Dordrecht
Duffield WA, Ruiz J (1998) A model that helps explain Sr-isotope disequilibrium between feldspar phenocrysts and melt in large-volume silicic magma systems. J Volcanol Geotherm Res 87:7–13
Duffield WA, Ruiz J, Webster JD (1995) Roof-rock contamination of magma along the top of the reservoir for the Bishop Tuff. J Volcanol Geotherm Res 69:187–195
Dunbar NW, Hervig RL (1992) Petrogenesis and volatile stratigraphy of the Bishop Tuff – evidence from melt inclusion analysis. J Geophys Res 97:15129–15150
Eberl DD, Drits VA, Srodon J (1998) Deducing growth mechanisms for minerals from the shapes of crystal size distributions. Am J Sci 298:499–533
Farver JR, Yund RA (1991) Oxygen diffusion in quartz: dependence on temperature and water fugacity. Chem Geol 90:55–70
Francis PW, Sparks RSJ, Hawkesworth CJ, Thorpe RS, Pyle DM, Tait SR, Mantovani MS, McDermott F (1989) Petrology and geochemistry of volcanic rocks of the Cerro Galan caldera, northwest Argentina. Geol Mag 126:515–547
Frost BR, Lindsley DH (1992) Equilibria among Fe–Ti oxides, pyroxenes, olivine, and quartz. Part II: application. Am Mineral 77:1004–1020
Giletti BJ (1991) Rb and Sr diffusion in feldspars, with implications for cooling histories of rocks. Geochim Cosmochim Acta 55:1331–1343
Goff F, Wollenberg HA, Brookins DC, Kistler RW (1991) A Sr-isotopic comparison between thermal waters, rocks, and hydrothermal calcites, Long Valley caldera, California. J Volcanol Geotherm Res 48:265–281
Halliday AN, Fallick AE, Hutchinson J, Hildreth W (1984) A Nd, Sr, and O isotopic investigation into causes of chemical and isotopic zonation in the Bishop Tuff, California. Earth Planet Sci Lett 68:378–391
Halliday AN, Mahood GA, Holden P, Metz JM, Dempster TJ, Davidson JP (1989) Evidence for long residence times of rhyolitic magma in the Long Valley magmatic system: the isotopic record in precaldera lavas of Glass Mountain. Earth Planet Sci Lett 94:274–290
Hervig RL, Dunbar NW (1992) Cause of chemical zoning in the Bishop (California) and Bandelier (New Mexico) magma chambers. Earth Planet Sci Lett 111:97–108
Heumann A (1999) Timescales of processes within silicic magma chambers. PhD Thesis, Netherlands Research School for Sedimentary Geology, Vrije Universiteit, Publication no 991001
Heumann A, Davies GR (1997) Isotopic and chemical evolution of the post-caldera rhyolitic system at Long Valley, California. J Petrol 38:1661–1678
Hildreth W (1979) The Bishop Tuff: evidence for the origin of compositional zonation in silicic magma chambers In: Chapin CE, Elston WE (eds) Geol Soc Am Spec Pap 180:43–75
Hildreth W, Mahood GA (1986) Ring-fracture eruption of Bishop Tuff. Geol Soc Am Bull 97:396–403
Hildreth W, Moorbath S (1988) Crustal contributions to arc magmatism in the Andes of Central Chile. Contrib Mineral Petrol 98:455–489
Hildreth W, Christiansen RL, O'Neil JR (1984) Catastrophic isotopic modification of rhyolitic magma at times of caldera subsidence, Yellowstone Plateau Volcanic Field. J Geophys Res 89:8339–8369
Holt EW, Taylor HP (1998) $^{18}O/^{16}O$ mapping and hydrogeology of a short-lived (approximately 10 years) fumarolic (> 500 degrees C) meteoric-hydrothermal event in the upper part of the 0.76 Ma Bishop Tuff outflow sheet, California. J Volcanol Geotherm Res 83:115–139
Knesel KM, Davidson JP (1997) The origin and evolution of large-volume silicic magma systems: Long Valley Caldera. Int Geol Rev 39:1033–1052
Lackey JS, Valley JW (1999) $\delta^{18}O$ and $\delta^{13}C$ evidence for infiltration-driven contact metamorphism of calcareous sandstone, Mt. Morrison Pendant, Long Valley, CA. Geol Soc Am Abstr 32:295
Liang Y, Richter FM, Davis AM, Watson EB (1996) Diffusion in silicate melts 1. Self diffusion in $CaO–Al_2O_3–SiO_2$ at 1,500 °C and 1 GPa. Geochim Cosmochim Acta 60:4353–4367
Lindsley DH, Frost RB, Ghiorso MS, Sack RO (1991) Oxides lie: the Bishop Tuff did not erupt from a thermally zoned magma body. Eos Trans AGU 72:312
Lipman PW (1984) The roots of ash flow calderas in western North America; windows into the tops of granitic batholiths. J Geophys Res 89:8801–8841
Lipman PW (1997) Subsidence of ash-flow calderas: relation to caldera size and magma-chamber geometry. Bull Volcanol 59:198–218
Lipman PW, Dungan M, Bachmann O (1997) Comagmatic granophyric granite in the Fish Canyon Tuff, Colorado: implications for magma-chamber processes during a large ash-flow eruption. Geology 25:915–918
Lu F (1991) The Bishop Tuff: origins of the high-silica rhyolite and its thermal and chemical zonations. PhD Thesis, University of Chicago
Mahood GA (1990) Second reply to the Comments of RSJ Sparks, HE Huppert, and CJN Wilson on "Evidence for long-residence times of rhyolitic magma in the Long Valley magmatic system: the isotopic record in precaldera lavas of Glass Mountain". Earth Planet Sci Lett 99:395–399
Mahood GA, Ring JH, McWilliams MO (2000) Contemporaneous mafic and silicic eruptions during the past 160 ka at Long Valley Caldera, CA: implications of new $^{40}Ar/^{39}Ar$ eruption ages for current volcanic hazards. Am Geophys Union Annu Meeting 1321
Mankinen EA, Gromme CS, Dalrymple GB, Lanphere MA, Bailey RA (1986) Paleomagnetism and K–Ar ages of volcanic rocks from Long Valley caldera, California. J Geophys Res 91:633–652
Masi U, O'Neil JR, Kistler RW (1981) Stable isotope systematics in Mesozoic granites of central and northern California and southwestern Oregon. Contrib Mineral Petrol 76:116–126
Matthews A, Palin JM, Epstein S, Stolper EM (1994) Experimental-study of $^{18}O/^{16}O$ partitioning between crystalline albite, albitic glass, and CO_2 gas. Geochim Cosmochim Acta 58:5255–5266
McBirney AR (1985) Further considerations of double-diffusive stratification and layering in the Skaergaard Intrusion. J Petrol 26:993–1001
McConnell VS, Shearer CK, Eichelberger JC, Keskinen MJ, Layer PW, Papike JJ (1995) Rhyolite intrusions in the intracaldera Bishop Tuff, Long Valley Caldera, California. J Volcanol Geotherm Res 67:41–60
McConnell VS, Valley JW, Eichelberger JC (1997) Oxygen isotope compositions of intracaldera rocks: hydrothermal history of the Long Valley Caldera, California. J Volcanol Geotherm Res 76:83–109
Metz JM, Bailey RA (1993) Geologic map of Glass Mountain, Mono County, California. US Geological Survey Misc Inv Series, Map I-1995, 1:24,000

Metz JM, Mahood GA (1991) Development of the Long Valley, California, magma chamber recorded in precaldera rhyolite lavas of Glass Mountain. Contrib Mineral Petrol 106:379–397

Nemchin AA, Giannini LM, Bodorkos S, Oliver NHS (2001) Ostwald ripening as a possible mechanism for zircon overgrowth formation during anatexis: theoretical constraints, a numerical model, and its application to pelitic migmatites of the Tickalara Metamorphics, northwestern Australia. Geochim Cosmochim Acta 65:2771–2788

Oldenburg CM, Spera FJ, Yuen DA, Sewell G (1989) Dynamic mixing in magma bodies: theory, simulations, and implications. J Geophys Res 94(B7):9215–9236

Palin JM, Epstein S, Stolper EM (1996) Oxygen isotope partitioning between rhyolitic glass/melt and CO_2: an experimental study at 550–950 degrees C and 1 bar. Geochim Cosmochim Acta 60:1963–1973

Peppard BT, Steele IM, Davis AM, Wallace PJ, Anderson AT (2001) Zoned quartz phenocrysts from the rhyolitic Bishop Tuff. Am Mineral 86:1034–1052

Reid MR, Coath CD (2000) In situ U–Pb ages of zircons from the Bishop Tuff: no evidence for long crystal residence times. Geology 28:443–446

Sarna-Wojcicki AM, Pringle MS, Wijbrans J (2000) New $^{40}Ar/^{39}Ar$ age of the Bishop Tuff from multiple sites and sediment rate calibration for the Matuyama–Brunhes boundary. J Geophys Res 105:21431–21443

Self S, Goff F, Gardner JN, Wright JV, Kite WM (1986) Explosive rhyolitic volcanism in the Jemez Mountains – vent locations, caldera development and relation to regional structure. J Geophys Res 91 (B2):1779–1798

Smith BM, Suemnicht GA (1991) Oxygen isotope evidence for past and present hydrothermal regimes of long valley caldera, California. J Volcanol Geotherm Res 48:319–339

Sparks RSJ, Huppert HE, Wilson CJN (1990) Comment on ''Evidence for long residence times of rhyolitic magma in the Long Valley magmatic system: the isotopic record in precaldera lavas of Glass Mountain''. Earth Planet Sci Lett 99:387–389

Spell TL, Kyle PR, Baker J (1996) Geochronology and geochemistry of the Cerro Toledo rhyolite. New Mexico Geol Surv Guidebook, 47th field conference, Jemez Mt. Region, pp 263–268

Spera FJ, Yuen DA, Clark S, Hong H-J (1987) Double-diffusive convection in magma chambers: single or multiple layers? Geophys Res Lett 13:153–156

Spicuzza MJ, Valley JW, McConnell VS (1998a) Oxygen isotope analysis of whole rocks via laser fluorination: an airlock approach. Geol Soc Am Abstr Program 30:80

Spicuzza MJ, Valley JW, Kohn MJ, Girard JP, Fouillac AM (1998b) The rapid heating, defocused beam technique: a CO_2-laser-based method for highly precise and accurate determination of $\delta^{18}O$ values of quartz. Chem Geol 144:195–203

Stanton T, Holloway J, Hervig RL (1989) Oxygen diffusion in hydrous silicate melts: resolution of the role of water speciation in the concentration dependence of water diffusion. EOS 70:501

Steinberg GS, Steinberg AS, Merzhanov AG (1989) Fluid mechanism of pressure growth in volcanic (magmatic) systems. Modern Geol 13:257–265

Stolper EM, Epstein S (1991)An experimental study of oxygen isotope partitioning between silica glass and CO_2 vapor. In: Taylor HP, O'Neil JR, Kaplan IR (eds). Geochem Soc Spec Publ 3:35–51

Swanson SE, Fenn PM (1986) Quartz crystallization in igneous rocks Am Mineral 71:331–342

Tinker D, Lesher CE (2001) Self diffusion of Si and O in dacitic liquid at high pressures Am Mineral 86:1–13

Trial AF, Spera FJ (1990) Mechanisms for the generation of compositional heterogeneities in magma chambers. Geol Soc Am Bull 102:353–367

Turner JS, Campbell IH (1986) Convection and mixing in magma chambers. Earth-Sci Rev 23:255–352

Valley JW, Kitchen N, Kohn MJ, Niendorf CR, Spicuzza MJ (1995) UWG-2, a garnet standard for oxygen isotope ratio: strategies for high precision and accuracy with laser heating. Geochim Cosmochim Acta 59:5223–5231

Wallace P, Anderson AT, Davis AM (1999) Gradients in H_2O, CO_2, and exsolved gas in a large-volume silicic magma system; interpreting the record preserved in melt inclusions from Bishop Tuff. J Geophys Res B104:20097–20122

Watson EB (1996) Dissolution, growth and survival of zircons during crustal fusion: kinetic principles, geologic models and implications for isotopic inheritance. Trans R Soc Edinb 87:43–56

Watson EB, Cherniak DJ (1997) Oxygen diffusion in zircon. Earth Planet Sci Lett 148:527–544

Watson EB, Harrison TM (1983) Zircon saturation revisited: temperature and compositional effects in a variety of crustal magma types. Earth Planet Sci Lett 64:295–304

Wendlandt RF (1991) Oxygen diffusion in basalt and andesite melts – experimental results and discussion of chemical versus tracer diffusion. Contrib Mineral Petrol 108:463–471

Wilson CJN, Hildreth W (1997) The Bishop Tuff: new insights from eruptive stratigraphy. J Geol 105:407–439

Winick JA, McIntosh WC, Dunbar NW (2001) Melt-inclusion-hosted excess Ar-40 in quartz crystals of the Bishop and Bandelier magma systems. Geology 29:275–278

Wolff JA, Ramos FC, Davidson JP (1999) Sr isotope disequilibrium during differentiation of the Bandelier Tuff: constraints on the crystallization of a large rhyolitic magma chamber. Geology 27:495–498

Zhang Y, Stolper EM, Wasserburg GI (1991) Diffusion of multispecies component and its role in oxygen and water transport in silicates. Earth Planet Sci Lett 103:228–240